

INTRUSIVE AND NON-INTRUSIVE REDUCED ORDER MODELING OF THE ROTATING THERMAL SHALLOW WATER EQUATION

A PREPRINT

✉ **Süleyman Yıldız**

Institute of Applied Mathematics
Middle East Technical University, Ankara-Turkey
yildiz.suleyman@metu.edu.tr

✉ **Bülent Karasözen**

Institute of Applied Mathematics & Department of Mathematics
Middle East Technical University, Ankara-Turkey
bulent@metu.edu.tr

✉ **Murat Uzunca**

Department of Mathematics
Sinop University, Sinop-Turkey
muzunca@sinop.edu.tr

ABSTRACT

In this paper, we investigate projection-based intrusive and data-driven non-intrusive model order reduction methods in numerical simulation of rotating thermal shallow water equation (RTSWE) in parametric and non-parametric form. Discretization of the RTSWE in space with centered finite differences leads to Hamiltonian system of ordinary differential equations with linear and quadratic terms. The full-order model (FOM) is obtained by applying linearly implicit Kahan's method in time. Applying proper orthogonal decomposition with Galerkin projection (POD-G), we construct the intrusive reduced-order model (ROM). We apply operator inference (OpInf) with re-projection for non-intrusive reduced-order modeling. In the parametric case, we make use of the parameter dependency at the level of the PDE without interpolating between the reduced operators. The least-squares problem of the OpInf is regularized with the minimum norm solution. Both ROMs behave similar and are able to accurately predict the test and training data and capture system behavior in the prediction phase with several orders of computational speedup over the FOM. The preservation of system physics such as the conserved quantities of the RTSWE by both ROMs enables that the models fit better to data and stable solutions are obtained in long-term predictions, which are robust to parameter changes.

Keywords Shallow water equation · Reduced order modeling · Proper orthogonal decomposition · Operator inference

1 Introduction

Rotating shallow water equation (RSWE) [Salmon(2004)] is used as conceptual and predictive model in geophysical fluid dynamics for the behavior of rotating inviscid fluids and has been applied to a diverse range of oceanographic and atmospheric phenomena. To describe three dimensional flows, multilayer RSWE model is used, where the fluid is discretized horizontally into a set of vertical layers, each having its own height, density and horizontal velocity. However, the RSWE model does not allow for gradients of the mean temperature and/or density. The rotating thermal shallow water equation (RTSWE) [Dellar(2003), Warneford and Dellar(2013), Eldred et al.(2019)Eldred, Dubos, and Kritsikis, Ripa(1995)] represents an extension of the RSWE equation, to include horizontal density/temperature gradients both in the atmospheric and oceanic context. The RTSWE is used in the general circulation models [Zerroukat and Allen(2015)], planetary flows [Warneford and Dellar(2014)], and modeling atmospheric and oceanic temperature fronts [Dempsey and Rotunno(1988), Young and Chen(1995)], thermal instabilities [Gouzien et al.(2017)Gouzien, Lahaye, Zeitlin, and Dubos].

High fidelity full order models (FOMs) for partial differential equations (PDEs) such as the shallow water equations (SWEs) are obtained with the standard discretization methods, e.g., finite-differences, finite-volumes, finite-elements, spectral elements, or discontinuous Galerkin methods. The computational cost associated with fully resolved solutions remains a barrier in real-time simulations on fine space-time grids. The dynamics of large-scale dynamical systems such as the SWEs typically lie in a low-dimensional space. Model order reduction (MOR) aims to construct low-dimensional and efficient reduced-order models (ROMs) to accurately approximate the underlying FOMs, which requires repeated evaluations of the model over a range of parameter values. Additionally, ROMs are even more valuable for SWEs in simulating and predicting the model over a long time horizon. The ROMs are implemented using the offline-online approach. The reduced basis functions are extracted from the snapshots in the offline stage, and the reduced basis is computed by combining them. In the online phase, the full problem is projected onto the reduced space, and the solutions for new parameters are computed in an efficient manner. Based on the offline-online methodology, there exists two versions of ROM methods; the intrusive and non-intrusive ones. In the case of intrusive ROM methods, the reduced solutions are determined by solving a reduced order model, i.e., a projection of the FOM onto the reduced space. The proper orthogonal decomposition (POD) with the Galerkin projection (POD-G) [Berkooz et al.(1993)Berkooz, Holmes, and Lumley, Sirovich(1987)] is arguably one of the most popular intrusive ROM methods. Applying the singular value decomposition (SVD) to the snapshot matrix, the POD basis are extracted. Then, ROM is constructed by applying Galerkin projection. For PDEs with only linear and polynomial terms like the SWEs, the projection-based reduced model admits an efficient low-dimensional numerical representation independent of the dimension of the FOM without necessitating hyper-reduction techniques like empirical/discrete empirical interpolation method [Barrault et al.(2004)Barrault, Maday, Nguyen, and Patera, Chaturantabut and Sorensen(2010)]. We refer to the books [Benner et al.(2017)Benner, Cohen, Ohlberger, and Willcox, Quarteroni and Rozza(2014), Schilders et al.(2021)Schilders, Grivet-Talocia, Benner, Quarteroni, Rozza, and Silveira] for an overview of the available MOR techniques.

Traditionally, projection-based model reduction is intrusive since the numerical implementation of the reduced models require access to the discretized PDE operators. The intrusive nature of MOR techniques limits the scope of traditional model reduction methods. The major drawback of intrusive methods is that they require access to the full model and solvers are typically unavailable when working with, and thus the traditional intrusive model reduction methods are not applicable when proprietary software is used for solving the PDEs, where the details of the governing equations are not known. Another class of ROMs is the data-driven or non-intrusive ROMs, which are fundamentally different from the intrusive ROMs. Unlike intrusive, using the non-intrusive model reduction techniques, reduced models are learnt from snapshots, i.e., either numerical approximations or measurements of the states of the dynamical systems, when the operators of the discretized systems are not available. There exist several software packages that are able to simulate SWEs for a given parameter set and an initial condition [Gibson et al.(2019)Gibson, McRae, Cotter, Mitchell, and Ham, Delestre et al.(2017)Delestre, Darboux, James, Lucas, Laguerre, and Cordier].

Machine learning plays an important role in analyzing the underlying process of the dynamics from the data. Recent advances in machine learning techniques such as neural networks offer new opportunities to develop more efficient and accurate ROMs. They learn a model based on the training data that neither requires explicit access to the high-fidelity model operators nor any additional information about the process. However, the amount of data required to learn the model accurately imposes a burden in the context of large-scale PDE simulations [Swischuk et al.(2019)Swischuk, Mainini, Peherstorfer, and Willcox]. Incorporating existing knowledge about the physics of the models requires less training data. We review the most relevant literature about learning dynamical-system models from data related to this work. Data-driven reduced models are constructed in the Loewner framework from input-output measurements by fitting linear-time invariant models to frequency or time-domain data [Ionita and Antoulas(2014), Peherstorfer et al.(2017)Peherstorfer, Gugercin, and Willcox]. The Loewner approach has been extended to bilinear [Antoulas et al.(2016)Antoulas, Gosea, and Ionita] and quadratic-bilinear systems [Gosea and Antoulas(2018)]. Dynamic mode decomposition (DMD) learns reduced models for nonlinear dynamical systems, by fitting linear operators to state trajectories with respect to the L_2 norm [Rowley et al.(2009)Rowley, Mezić, Bagheri, Schlatter, and Henningson, Schmid(2010)]. Methods based on the Koopman operator has been developed to extend DMD to nonlinear dynamical systems [Williams et al.(2015)Williams, Kevrekidis, and Rowley]. Reduced models are also constructed in the high-dimensional systems by exploiting sparsity [Brunton et al.(2016)Brunton, Proctor, and Kutz, Loiseau and Brunton(2018), Schaeffer et al.(2018)Schaeffer, Tran, and Ward]. Recently, data-fit surrogate models with artificial neural networks (ANNs) are used as the regression models for the non-intrusive ROMs for time-dependent dynamical systems [Hesthaven and Ubbiali(2018), Wang et al.(2019)Wang, Hesthaven, and Ray].

In recent years, the operator inference (OpInf) method to construct ROMs non-intrusively has gained much attention, which was first investigated for polynomial nonlinearities in [Peherstorfer and Willcox(2016)]. The operators

defining the ROM can be learned by formulating an optimization problem, i.e., least-squares problem without accessing the discretized operators of the PDEs. The methodology was later extended to nonlinear systems that can be written as a polynomial or quadratic-bilinear system by utilizing lifting variable transformation, called Lift & Learn method [Kramer and Willcox(2019), Qian et al.(2020)Qian, Kramer, Peherstorfer, and Willcox]. In [Benner et al.(2020a)Benner, Goyal, Kramer, Peherstorfer, and Willcox], OpInf method is applied to nonlinear systems in which the structure of the nonlinearities is preserved while learning ROMs from data. Data-driven ROMs via regularized OpInf are employed to combustion problems [McQuarrie et al.(2021)McQuarrie, Huang, and Willcox, Swischuk et al.(2020)Swischuk, Kramer, Huang, and Willcox]. The OpInf method is also used for data-driven reduced-order modeling in fluid dynamics; such as incompressible flows [Benner et al.(2020b)Benner, Goyal, Heiland, and Duff] and SWEs [Yildiz et al.(2020)Yildiz, Goyal, Benner, and Karasözen]. Recently in [Qian et al.(2021)Qian, Farcas, and Willcox], the OpInf method is generalized to the PDE setting through the use of lifting variables. In the case of linear FOMs, the OpInf method equivalent to the DMD, the inferred operators are the same. Recently the DMD is extended to quadratic bilinear systems [Gosea and Duff(2020)]. When the future states of dynamical systems depend only on the current state and not on previous ones, they are called Markovian systems. The non-Markovian systems are considered having a memory, where future states depend on the current and previous states. The projected trajectories of the OpInf [Peherstorfer and Willcox(2016)] correspond to non-Markovian dynamics in the low-dimensional subspaces even though the FOMs are Markovian, as known from, e.g., the Mori–Zwanzig formalism [Chorin and Stinis(2006), Givon et al.(2004)Givon, Kupferman, and Stuart]. The non-Markovian dynamics has been investigated intensively [Gouasmi et al.(2017)Gouasmi, Parish, and Duraisamy, Mou et al.(2021)Mou, Koc, San, Rebholz, and Iliescu, Fick et al.(2018)Fick, Maday, Patera, and Taddei, Rahman et al.(2019)Rahman, Ahmed, and San, Wang et al.(2020)Wang, Ripamonti, and Hesthaven]. To recover the Markovian dynamics of the reduced system, a data sampling scheme has devised in [Peherstorfer(2020)], which iterates between time stepping the high-dimensional FOM and projecting onto low-dimensional reduced subspaces. In this way the Markovian dynamics is retained in low-dimensional subspaces. It was shown in [Peherstorfer(2020)] that under certain conditions, applying operator inference to re-projected trajectories for dynamical systems with polynomial nonlinear terms, produces the same operators that are obtained with the intrusive model reduction methods. Recently, probabilistic a posteriori error estimators are derived for the OpInf with re-projection for linear parabolic PDEs [Tan Uy and Peherstorfer(2020)] and a non-Markovian OpInf with partial information is investigated [Uy and Peherstorfer(2021)]. A deep learning version of the OpInf is introduced in [Goyal and Benner(2021)].

Intrusive and non-intrusive MOR techniques, POD-G and DMD have been intensively studied for the SWEs, see e.g., [Bistrian and Navon(2015), Bistrian and Navon(2017), Esfahanian and Ashrafi(2009), Karasözen et al.(2021)Karasözen, Yıldız, and Uzunca, Lozovskiy et al.(2016)Lozovskiy, Farthing, Kees, and Gildin, Lozovskiy et al.(2017)Lozovskiy, Farthing, and Kees, Ahmed et al.(2020)Ahmed, San, Bistrian, and Navon, Ștefănescu et al.(2014)Ștefănescu, Sandu, and Navon]. In this paper, we present efficient ROMs by applying the intrusive POD-G and the non-intrusive data-driven OpInf method to the RTSWE in the parametric and non-parametric forms. The RTSWE is discretized in space with the second-order centered finite differences while preserving the Hamiltonian structure, which leads to a linear-quadratic system of ordinary differential equations (ODEs). For time discretization we use the linearly implicit Kahan’s method which is designed for linear-quadratic ODE systems like the RTSWE in the semi-discrete form. It is second-order accurate in time, and has a lower computational cost than the fully implicit schemes such as the Crank-Nicolson scheme. Kahan’s method requires only one step Newton iteration at each time level. Furthermore, it has favorable conservation properties; the energy (Hamiltonian) and other conserved quantities of the RTSWE like the mass, the total vorticity, and the buoyancy are preserved in long-time integration. To accelerate the online and offline ROM computations, we apply the POD-G by the use of matricization of tensors [Benner et al.(2018)Benner, Goyal, and Gugercin, Benner and Goyal(2021), Karasözen et al.(2021)Karasözen, Yıldız, and Uzunca] and the sparse matrix technique MULTIPROD [Leva(2008)]. We apply the OpInf with re-projection [Peherstorfer(2020)] to the RTSWE by preserving the low-dimensional Markovian dynamics. It was shown through by the numerical results that learning low-dimensional models with the OpInf method with re-projection [Peherstorfer(2020)] are very close to the reduced models from intrusive model reduction POD-G. The energy and other conserved quantities are well preserved with the POD-G and OpInf without any drift over time. We compare POD-G with the OpInf method for the parametric case with the Coriolis force, where we make use of the known parametric dependency at the PDE level, whereas in [Peherstorfer and Willcox(2016), Peherstorfer(2020)] the ROMs are constructed at each training parameter via interpolation. We show that under certain assumptions on the time discretization [Peherstorfer and Willcox(2016), Peherstorfer(2020)] the intrusive POD-G model converges to the learned non-intrusive OpInf model. Numerical results also show that both the POD-G and the OpInf methods can predict the reduced parametric models with high accuracy. Furthermore, we show that the ROMs exhibit high accuracy in the training regime and acceptable accuracy in prediction phase. The data matrices in the least-squares problem of the

OpInf have large condition numbers, leading to ill-conditioned inverse problem. To deal with this issue, regularization techniques like the truncated SVD or Tikhonov regularization should be used. Because, decay of the singular values of the data matrices does not provide any information about the choice of the tolerance for the regularization parameter, we solve the least-squares problem in the minimum norm, where the tolerances are determined with the L-curve. Speed-up factors of order two over the FOM are achieved for both ROMs, whereas the OpInf is more costly than the POD-G due to the re-projection.

The paper is organized as follows. In Section 2, the RTSWE and the full space-time discretization are described. The detailed formulations of intrusive POD-G and the non-intrusive OpInf are given in Section 3. In Section 4, numerical results are presented for the double vortex RTSWE in the non-parametric and in the parametric form, and for prediction over a time horizon. The paper ends with some concluding remarks in Section 5.

2 Rotating Thermal Shallow Water Equation

RSWE [Salmon(2004), Salmon(2007)] is considered in rotating inviscid fluids with one or more layers [Stewart and Dellar(2016)], within each layer the horizontal velocity is assumed to be depth-independent, so the fluid moves in columns. Large-scale vortex and wave dynamics can be understood with this model [Zeitlin(2018)]. However, a drawback of this model is that it does not admit horizontal temperature and density gradients. The RTSWE represents an extension of the RSWE allowing for gradients in the atmospheric and oceanic context, known also as Ripa equation [Ripa(1995)]. It is obtained along the same lines as the RSWE, using the hypothesis of columnar motion, but with nonuniform density/temperature [Gouzien et al.(2017)Gouzien, Lahaye, Zeitlin, and Dubos, Zeitlin(2018)]. Typical applications of the RTSWE are to model atmospheric and oceanic temperature fronts, mixed boundary layers [Young and Chen(1995)]. RTSWE is given for the primitive variables [Warneford and Dellar(2013), Eldred et al.(2019)Eldred, Dubos, and Kritsikis] as

$$\begin{aligned}\frac{\partial h}{\partial t} &= -(hu)_x - (hv)_y, \\ \frac{\partial u}{\partial t} &= hqv - \left(\frac{u^2 + v^2}{2}\right)_x - \frac{h}{2}s_x - s(h+b)_x, \\ \frac{\partial v}{\partial t} &= -hqu - \left(\frac{u^2 + v^2}{2}\right)_y - \frac{h}{2}s_y - s(h+b)_y, \\ \frac{\partial s}{\partial t} &= -us_x - vs_y,\end{aligned}\tag{1}$$

where $u(x, y, t)$ and $v(x, y, t)$ are the relative velocities, $h(x, y, t)$ is the fluid height, $b(x, y)$ topographic height, $\rho(x, y, t)$ fluid density, g gravity constant, $s = g\frac{\rho}{\rho_0}$ the buoyancy, $S = hs$ mass-weighted buoyancy, and $q = (v_x - u_y + f)/h$ is the potential vorticity with the Coriolis parameter $f(\mu) = 2\Omega \sin(\mu)$, where μ varies with the latitude and $\Omega = 7.292 \times 10^{-5}$ is the rotational speed of the Earth. The standard RSWE is recovered in the limit of constant density, i.e., constant buoyancy.

The RTSWE (1) is considered on a rectangular domain $\Omega = [a, b] \times [c, d]$ with periodic boundary conditions, and on a time interval $[0, T]$ for a target time $T > 0$, together with the given initial conditions

$$u(\mathbf{x}, 0) = u_0(\mathbf{x}), \quad v(\mathbf{x}, 0) = v_0(\mathbf{x}), \quad h(\mathbf{x}, 0) = h_0(\mathbf{x}), \quad s(\mathbf{x}, 0) = s_0(\mathbf{x}).$$

The RTSWE is a non-canonical Hamiltonian PDE with state-dependent Poisson matrix [Dellar(2002), Warneford and Dellar(2013), Eldred et al.(2019)Eldred, Dubos, and Kritsikis]. The conserved Hamiltonian or energy is given by

$$\mathcal{E}(z) = \int_{\Omega} \left(\frac{h^2 s}{2} + hsb + h \frac{u^2 + v^2}{2} \right) d\Omega.\tag{2}$$

Other conserved quantities are the Casimirs: the mass, the total potential vorticity, and the buoyancy defined respectively by

$$\mathcal{M} = \int_{\Omega} h \, d\Omega, \quad \mathcal{Q} = \int_{\Omega} q \, d\Omega, \quad \mathcal{B} = \int_{\Omega} hs \, d\Omega.\tag{3}$$

The RTSWE (1) is discretized by finite differences on a uniform grid of the rectangular spatial domain $\Omega = [a, b] \times [c, d]$ with the nodes $\mathbf{x}_{ij} = (x_i, y_j)^T$, where $x_i = a + (i-1)\Delta x$, $y_j = c + (j-1)\Delta y$, $i, j = 1, \dots, n+1$, and spatial

mesh sizes are $\Delta x = (b - a)/n$ and $\Delta y = (d - c)/n$. Using the from bottom to top/from left to right ordering of the grid nodes, the vectors of semi-discrete state variables are defined as

$$\begin{aligned} \mathbf{h}(t) &= (h_{1,1}(t), \dots, h_{1,n}(t), h_{2,1}(t), \dots, h_{2,n}(t), \dots, h_{n,n}(t))^T, \\ \mathbf{u}(t) &= (u_{1,1}(t), \dots, u_{1,n}(t), u_{2,1}(t), \dots, u_{2,n}(t), \dots, u_{n,n}(t))^T, \\ \mathbf{v}(t) &= (v_{1,1}(t), \dots, v_{1,n}(t), v_{2,1}(t), \dots, v_{2,n}(t), \dots, v_{n,n}(t))^T, \\ \mathbf{s}(t) &= (s_{1,1}(t), \dots, s_{1,n}(t), s_{2,1}(t), \dots, s_{2,n}(t), \dots, s_{n,n}(t))^T, \end{aligned} \quad (4)$$

where we set $w_{i,j}(t) = w(x_i, y_j, t)$ for $w = h, u, v, s$. We note that the degree of freedom (dimension of FOM) is given by $N := n^2$ because of the periodic boundary conditions, i.e., the most right grid nodes $\mathbf{x}_{n+1,j}$ and the most top grid nodes $\mathbf{x}_{i,n+1}$ are not included. The solution vector is defined by $\mathbf{z}(t) = (\mathbf{h}(t), \mathbf{u}(t), \mathbf{v}(t), \mathbf{s}(t)) : [0, T] \mapsto \mathbb{R}^{4N}$. Throughout the paper, we do not explicitly represent the time dependency of the semi-discrete solutions for simplicity, and we write $\mathbf{u}, \mathbf{v}, \mathbf{h}, \mathbf{s}$, and \mathbf{z} .

The first-order derivatives in space are approximated by utilizing one-dimensional centered finite differences in x and y directions, and they are extended to two dimensions by the use of the Kronecker product. Let $\tilde{D}_n \in \mathbb{R}^{n \times n}$ be the matrix corresponding to the centered finite differences under periodic boundary conditions on a one-dimensional domain (interval)

$$\tilde{D}_n = \begin{pmatrix} 0 & 1 & & & -1 \\ -1 & 0 & 1 & & \\ & \ddots & \ddots & \ddots & \\ & & -1 & 0 & 1 \\ 1 & & & 1 & 0 \end{pmatrix}.$$

Then, on the two dimensional mesh, the centered finite difference matrices $D_x \in \mathbb{R}^{N \times N}$ and $D_y \in \mathbb{R}^{N \times N}$ corresponding to the first order partial derivatives ∂_x and ∂_y , respectively, can be calculated as

$$D_x = \frac{1}{2\Delta x} \tilde{D}_n \otimes I_n, \quad D_y = \frac{1}{2\Delta y} I_n \otimes \tilde{D}_n,$$

where \otimes denotes the Kronecker product, and I_n is the identity matrix of size n . Then, the semi-discretization of the RTSWE (1) leads to the following system of linear-quadratic ODEs

$$\begin{aligned} \frac{d\mathbf{h}}{dt} &= -D_x(\mathbf{u} \circ \mathbf{h}) - D_y(\mathbf{v} \circ \mathbf{h}), \\ \frac{d\mathbf{u}}{dt} &= -\mathbf{u} \circ (D_x \mathbf{u}) - \mathbf{v} \circ (D_y \mathbf{u}) - \frac{\mathbf{h}}{2} \circ D_x \mathbf{s} - \mathbf{s} \circ D_x \mathbf{h} - \mathbf{s} \circ D_x \mathbf{b} + f\mathbf{v}, \\ \frac{d\mathbf{v}}{dt} &= -\mathbf{u} \circ (D_x \mathbf{v}) - \mathbf{v} \circ (D_y \mathbf{v}) - \frac{\mathbf{h}}{2} \circ D_y \mathbf{s} - \mathbf{s} \circ D_y \mathbf{h} - \mathbf{s} \circ D_y \mathbf{b} - f\mathbf{u}, \\ \frac{d\mathbf{s}}{dt} &= -\mathbf{u} \circ D_x \mathbf{s} - \mathbf{v} \circ D_y \mathbf{s}. \end{aligned} \quad (5)$$

For $\mathbf{w} = (\mathbf{h}, \mathbf{u}, \mathbf{v}, \mathbf{s})$, the system (5) can be rewritten in the compact form as

$$\dot{\mathbf{w}} = \mathbf{F}(\mathbf{w}) = \mathbf{A}\mathbf{w} + \mathbf{H}(\mathbf{w} \otimes \mathbf{w}), \quad (6)$$

where $\dot{\mathbf{w}}$ denotes the time derivative of the state vector \mathbf{w} , and $\mathbf{A} \in \mathbb{R}^{4N \times 4N}$ is a linear matrix operator corresponding to the linear terms

$$\mathbf{A} = \begin{pmatrix} 0 & 0 & 0 & 0 \\ 0 & 0 & f\mathbf{I} & -(D_x \mathbf{b})^d \\ 0 & -f\mathbf{I} & 0 & -(D_y \mathbf{b})^d \\ 0 & 0 & 0 & 0 \end{pmatrix},$$

where $\mathbf{I} \in \mathbb{R}^{N \times N}$ is the identity matrix and $(D_x \mathbf{b})^d \in \mathbb{R}^{N \times N}$ is the diagonal matrix whose diagonal entries are given by the elements of the vector $D_x \mathbf{b}$, i.e., $((D_x \mathbf{b})^d)_{ii} = (D_x \mathbf{b})_i, i = 1, \dots, N$. The vector $\mathbf{H}(\mathbf{w} \otimes \mathbf{w}) \in \mathbb{R}^{4N}$ contains the quadratic terms

$$\mathbf{H}(\mathbf{w} \otimes \mathbf{w}) = \begin{pmatrix} -D_x(\mathbf{u} \circ \mathbf{h}) - D_y(\mathbf{v} \circ \mathbf{h}) \\ -\mathbf{u} \circ (D_x \mathbf{u}) - \mathbf{v} \circ (D_y \mathbf{u}) - \frac{\mathbf{h}}{2} \circ D_x \mathbf{s} - \mathbf{s} \circ D_x \mathbf{h} \\ -\mathbf{u} \circ (D_x \mathbf{v}) - \mathbf{v} \circ (D_y \mathbf{v}) - \frac{\mathbf{h}}{2} \circ D_y \mathbf{s} - \mathbf{s} \circ D_y \mathbf{h} \\ -\mathbf{u} \circ D_x \mathbf{s} - \mathbf{v} \circ D_y \mathbf{s} \end{pmatrix},$$

where \circ denotes the elementwise matrix or Hadamard product, and $\mathbf{H} \in \mathbb{R}^{4N \times (4N)^2}$ is an appropriate matricized tensor operator such that the right hand side of the above equality is obtained.

For time discretization, we partition the time interval $[0, T]$ into K uniform intervals with the step size $\Delta t = T/K$ as $0 = t_0 < t_1 < \dots < t_K = T$, and $t_k = k\Delta t$, $k = 0, 1, \dots, K$. Then, we denote by $\mathbf{w}^k = \mathbf{w}(t_k)$ the fully discrete solution vector at time t_k . For the linear-quadratic autonomous ODE system (6), we use Kahan's "unconventional" discretization [Kahan(1993)], which yields the system

$$\frac{\mathbf{w}^{k+1} - \mathbf{w}^k}{\Delta t} = \frac{1}{2} \mathbf{A} (\mathbf{w}^k + \mathbf{w}^{k+1}) + \bar{\mathbf{H}} ((\mathbf{w}^k \otimes \mathbf{w}^k), (\mathbf{w}^{k+1} \otimes \mathbf{w}^{k+1})),$$

where the symmetric bilinear form $\bar{\mathbf{H}}(\cdot, \cdot)$ denotes the polarization [Celledoni et al.(2015)Celledoni, McLachlan, McLaren, Owren, and Quispel] of the quadratic vector field $\mathbf{H}(\cdot)$, given by

$$\begin{aligned} \bar{\mathbf{H}} ((\mathbf{w}^k \otimes \mathbf{w}^k), (\mathbf{w}^{k+1} \otimes \mathbf{w}^{k+1})) &= \frac{1}{2} (\mathbf{H} ((\mathbf{w}^k + \mathbf{w}^{k+1}) \otimes (\mathbf{w}^k + \mathbf{w}^{k+1}))) \\ &\quad - \frac{1}{2} (\mathbf{H} (\mathbf{w}^k \otimes \mathbf{w}^k) + \mathbf{H} (\mathbf{w}^{k+1} \otimes \mathbf{w}^{k+1})). \end{aligned}$$

Kahan's method is second-order and time-reversal and linearly implicit for quadratic vector fields [Celledoni et al.(2013)Celledoni, McLachlan, Owren, and Quispel], i.e., it requires only one step of Newton iterations per time step

$$\left(I - \frac{\Delta t}{2} \mathbf{F}'(\mathbf{w}^k) \right) \frac{\mathbf{w}^{k+1} - \mathbf{w}^k}{\Delta t} = \mathbf{F}(\mathbf{w}^k), \quad (7)$$

where $\mathbf{F}'(\mathbf{w}^k)$ stands for the Jacobian matrix of $\mathbf{F}(\mathbf{w})$ evaluated at \mathbf{w}^k , and I is the identity matrix of size $4N$.

Under periodic boundary conditions, the full discrete forms of the energy, the mass, the total potential vorticity, and the buoyancy are given at the time instance t_k respectively as

$$\begin{aligned} H^k(\mathbf{w}) &= \sum_{i=1}^n \sum_{j=1}^n \left(\frac{1}{2} (h_{i,j}^k)^2 s_{i,j}^k + h_{i,j}^k s_{i,j}^k b_{i,j}^k + h_{i,j}^k \frac{(u_{i,j}^k)^2 + (v_{i,j}^k)^2}{2} \right) \Delta x \Delta y, \\ M^k(\mathbf{w}) &= \sum_{i=1}^n \sum_{j=1}^n h_{i,j}^k \Delta x \Delta y, \\ Q^k(\mathbf{w}) &= \sum_{i=1}^n \sum_{j=1}^n \left(\frac{v_{i+1,j}^k - v_{i-1,j}^k}{2\Delta x} - \frac{u_{i,j+1}^k - u_{i,j-1}^k}{2\Delta y} + f \right) \Delta x \Delta y, \\ B^k(\mathbf{w}) &= \sum_{i=1}^n \sum_{j=1}^n h_{i,j}^k s_{i,j}^k \Delta x \Delta y, \end{aligned} \quad (8)$$

where $b_{i,j}^k = b(x_i, y_j, t_k)$, and, for $w = h, u, v, s$, $w_{i,j}^k = w(x_i, y_j, t_k)$ are full discrete approximations at (x_i, y_j, t_k) satisfying $w_{i+n,j}^k = w_{i,j}^k$ and $w_{i,j+n}^k = w_{i,j}^k$ because of the periodic boundary conditions, $i, j = 1, \dots, n$.

Linear conserved quantities such as the mass are preserved by all Runge-Kutta type methods including Kahan's methods. Kahan's methods also preserves the quadratic and cubic polynomial invariants of Hamiltonian PDEs approximately over long times [Celledoni et al.(2015)Celledoni, McLachlan, McLaren, Owren, and Quispel, Eidnes et al.(2019)Eidnes, Li, and Sato]. The numerical errors in the conserved quantities of the RTSWE, such as the energy, vorticity and buoyancy have bounded oscillations over time.

3 Reduced order modeling

In this section the intrusive POD-G ROM and the non-intrusive ROM with the OpInf are constructed for the following parametric form of RTSWE (6)

$$\dot{\mathbf{w}}(t; \mu) = \mathbf{A}(\mu) \mathbf{w}(t; \mu) + \mathbf{H}(\mathbf{w}(t; \mu) \otimes \mathbf{w}(t; \mu)). \quad (9)$$

We remark that only the linear operator \mathbf{A} depends on the parameter $\mu \in \mathcal{D} \subset \mathbb{R}^d$, the operator \mathbf{H} in quadratic part is independent of the parameter.

We describe first the offline stage of constructing the POD basis, which is common for the intrusive and non-intrusive model reduction. The first step of the offline stage represents an initialization of a training set of parameters of

cardinality M . Then, in the second step, we query the FOM solutions for each parameter μ in the training set. To each parameter, it is associated a snapshot containing approximations of the state variables $\mathbf{h}, \mathbf{u}, \mathbf{v}, \mathbf{s}$ at each time step. In the third step, the information provided by the snapshots is compressed through the POD.

The reduced basis vectors are obtained usually by stacking all state variables in one vector and a common reduced subspace is computed by taking the SVD of the snapshot data. Because the governing PDEs like the RTSWE (1) are coupled, the resulting ROMs do not preserve the coupling topological structure of the FOM [Benner and Feng(2015), Reis and Stykel(2007)] and both intrusive and non-intrusive methods produce unstable ROMs [Qian et al.(2020)Qian, Kramer, Peherstorfer, and Willcox]. In order to maintain the coupling structure in ROMs, the POD basis vectors are computed separately for each state vector $\mathbf{h}, \mathbf{u}, \mathbf{v}, \mathbf{s}$. Let $W_h(\mu), W_u(\mu), W_v(\mu), W_s(\mu) \in \mathbb{R}^{N \times K}$ be the trajectories for each state vector and parameter μ

$$\begin{aligned} W_h(\mu) &= [\mathbf{h}^1(\mu) \cdots \mathbf{h}^K(\mu)], & W_u(\mu) &= [\mathbf{u}^1(\mu) \cdots \mathbf{u}^K(\mu)], \\ W_v(\mu) &= [\mathbf{v}^1(\mu) \cdots \mathbf{v}^K(\mu)], & W_s(\mu) &= [\mathbf{s}^1(\mu) \cdots \mathbf{s}^K(\mu)]. \end{aligned}$$

The corresponding global snapshot matrices of the concatenated trajectories and parameter values $\mu_1, \dots, \mu_M \in \mathcal{D}$ are given as

$$\begin{aligned} W_{h\mu} &= [W_h(\mu_1) \cdots W_h(\mu_M)], & W_{u\mu} &= [W_u(\mu_1) \cdots W_u(\mu_M)], \\ W_{v\mu} &= [W_v(\mu_1) \cdots W_v(\mu_M)], & W_{s\mu} &= [W_s(\mu_1) \cdots W_s(\mu_M)]. \end{aligned}$$

The POD basis are constructed by computing the SVD of the global snapshot matrix $W_\mu \in \mathbb{R}^{4N \times MK}$ for the semidiscrete RTSW equation (6) in the following form

$$W_\mu = \begin{pmatrix} W_{h\mu} \\ W_{u\mu} \\ W_{v\mu} \\ W_{s\mu} \end{pmatrix} = \begin{pmatrix} \Phi_h & & & \\ & \Phi_u & & \\ & & \Phi_v & \\ & & & \Phi_s \end{pmatrix} \begin{pmatrix} \Sigma_h & & & \\ & \Sigma_u & & \\ & & \Sigma_v & \\ & & & \Sigma_s \end{pmatrix} \begin{pmatrix} \Psi_h^T \\ \Psi_u^T \\ \Psi_v^T \\ \Psi_s^T \end{pmatrix}$$

with the orthonormal matrices $\Phi_h, \Phi_u, \Phi_v, \Phi_s \in \mathbb{R}^{N \times N}$, and $\Psi_h, \Psi_u, \Psi_v, \Psi_s \in \mathbb{R}^{MK \times N}$, and with the diagonal matrices $\Sigma_h, \Sigma_u, \Sigma_v, \Sigma_s \in \mathbb{R}^{N \times N}$ containing the singular values in descending order $\sigma_1 \geq \sigma_2, \dots$. The POD basis vectors $\Phi_{r_h}, \Phi_{r_u}, \Phi_{r_v}$ and Φ_{r_s} are given by the r_h, r_u, r_v and r_s leading columns of the matrices Φ_h, Φ_u, Φ_v and Φ_s , respectively, and yields the approximation

$$\begin{pmatrix} \mathbf{h} \\ \mathbf{u} \\ \mathbf{v} \\ \mathbf{s} \end{pmatrix} \approx \begin{pmatrix} \Phi_{r_h} & & & \\ & \Phi_{r_u} & & \\ & & \Phi_{r_v} & \\ & & & \Phi_{r_s} \end{pmatrix} \begin{pmatrix} \tilde{\mathbf{h}} \\ \tilde{\mathbf{u}} \\ \tilde{\mathbf{v}} \\ \tilde{\mathbf{s}} \end{pmatrix},$$

where $\tilde{\mathbf{h}}, \tilde{\mathbf{u}}, \tilde{\mathbf{v}}$ and $\tilde{\mathbf{s}}$ are the reduced coefficients. Although different number of modes can be used for each state, in the present study we use equal number of modes, i.e., $r = r_u = r_v = r_h = r_s$. Note that the POD basis are independent of the parameter $\mu \in \mathcal{D}$.

The deterministic SVD for the snapshot matrices of size $N \times K$ has asymptotic time complexity of $\mathcal{O}(\min(NK^2, N^2K))$. We use the randomized SVD (rSVD) [Halko et al.(2011)Halko, Martinsson, and Tropp, Bach et al.(2019)Bach, Ceglia, Song, and Duddeck] which is faster than the deterministic SVD for large matrices and has asymptotic complexity of only $\mathcal{O}(NKr)$.

3.1 Proper orthogonal decomposition with Galerkin projection

In the POD-G ROM, a reduced system is obtained by Galerkin projection of the FOM (6) onto the space spanned by the POD vectors

$$\Phi_r = \begin{pmatrix} \Phi_{r_h} & & & \\ & \Phi_{r_u} & & \\ & & \Phi_{r_v} & \\ & & & \Phi_{r_s} \end{pmatrix} \in \mathbb{R}^{4N \times 4r}.$$

After projection, the reduced system reads as

$$\dot{\tilde{\mathbf{w}}}(t; \mu) = \tilde{\mathbf{A}}(\mu) \tilde{\mathbf{w}}(t; \mu) + \tilde{\mathbf{H}}(\tilde{\mathbf{w}}(t; \mu) \otimes \tilde{\mathbf{w}}(t; \mu)), \quad (10)$$

where the reduced linear operator is given by

$$\tilde{\mathbf{A}}(\mu) = \Phi_r^T \mathbf{A}(\mu) \Phi_r = \begin{pmatrix} 0 & 0 & 0 & 0 \\ 0 & 0 & f(\mu) \Phi_{r_u}^T \Phi_{r_v} & -\Phi_{r_u}^T (D_x \mathbf{b})^d \Phi_{r_s} \\ 0 & -f(\mu) \Phi_{r_v}^T \Phi_{r_u} & 0 & -\Phi_{r_v}^T (D_y \mathbf{b})^d \Phi_{r_s} \\ 0 & 0 & 0 & 0 \end{pmatrix} \in \mathbb{R}^{4r \times 4r},$$

while the reduced quadratic operator is $\tilde{\mathbf{H}} = \Phi_r^T \mathbf{H}(\Phi_r \otimes \Phi_r) \in \mathbb{R}^{4r \times (4r)^2}$. We note that the linear-quadratic structure of the FOM (6) is preserved by the reduced system (10) (see [Benner and Breiten(2015)]) which is also solved in time by Kahan's method (7) as the FOM.

For computational aspects, we separate the quadratic term in (10) and we rewrite the intrusive ROM (10) in the following form

$$\begin{aligned} \dot{\tilde{\mathbf{w}}}(t; \mu) = & \tilde{\mathbf{A}}(\mu) \tilde{\mathbf{w}}(t; \mu) + \tilde{\mathbf{H}}_1 \begin{bmatrix} 0 \\ (\tilde{\mathbf{u}}(t; \mu) \otimes \tilde{\mathbf{u}}(t; \mu)) \\ (\tilde{\mathbf{v}}(t; \mu) \otimes \tilde{\mathbf{u}}(t; \mu)) \\ 0 \end{bmatrix} + \tilde{\mathbf{H}}_2 \begin{bmatrix} (\tilde{\mathbf{h}}(t; \mu) \otimes \tilde{\mathbf{u}}(t; \mu)) \\ (\tilde{\mathbf{v}}(t; \mu) \otimes \tilde{\mathbf{u}}(t; \mu)) \\ (\tilde{\mathbf{v}}(t; \mu) \otimes \tilde{\mathbf{v}}(t; \mu)) \\ (\tilde{\mathbf{s}}(t; \mu) \otimes \tilde{\mathbf{u}}(t; \mu)) \end{bmatrix} \\ & + \tilde{\mathbf{H}}_3 \begin{bmatrix} (\tilde{\mathbf{h}}(t; \mu) \otimes \tilde{\mathbf{v}}(t; \mu)) \\ (\tilde{\mathbf{h}}(t; \mu) \otimes \tilde{\mathbf{s}}(t; \mu)) \\ (\tilde{\mathbf{h}}(t; \mu) \otimes \tilde{\mathbf{s}}(t; \mu)) \\ (\tilde{\mathbf{s}}(t; \mu) \otimes \tilde{\mathbf{v}}(t; \mu)) \end{bmatrix} + \tilde{\mathbf{H}}_4 \begin{bmatrix} 0 \\ (\tilde{\mathbf{s}}(t; \mu) \otimes \tilde{\mathbf{h}}(t; \mu)) \\ (\tilde{\mathbf{s}}(t; \mu) \otimes \tilde{\mathbf{h}}(t; \mu)) \\ 0 \end{bmatrix}, \end{aligned} \quad (11)$$

where each reduced matrix $\tilde{\mathbf{H}}_i \in \mathbb{R}^{4r \times 4r^2}$, $i = 1, \dots, 4$, is in the block diagonal form defined by

$$\begin{aligned} \tilde{\mathbf{H}}_1 &= \begin{pmatrix} 0 & & & \\ & \tilde{\mathbf{H}}_1^1 & & \\ & & \tilde{\mathbf{H}}_1^2 & \\ & & & 0 \end{pmatrix}, \quad \tilde{\mathbf{H}}_2 = \begin{pmatrix} \tilde{\mathbf{H}}_2^1 & & & \\ & \tilde{\mathbf{H}}_2^2 & & \\ & & \tilde{\mathbf{H}}_2^3 & \\ & & & \tilde{\mathbf{H}}_2^4 \end{pmatrix}, \\ \tilde{\mathbf{H}}_4 &= \begin{pmatrix} 0 & & & \\ & \tilde{\mathbf{H}}_4^1 & & \\ & & \tilde{\mathbf{H}}_4^2 & \\ & & & 0 \end{pmatrix}, \quad \tilde{\mathbf{H}}_3 = \begin{pmatrix} \tilde{\mathbf{H}}_3^1 & & & \\ & \tilde{\mathbf{H}}_3^2 & & \\ & & \tilde{\mathbf{H}}_3^3 & \\ & & & \tilde{\mathbf{H}}_3^4 \end{pmatrix}, \end{aligned}$$

with the $r \times r^2$ matrices

$$\begin{aligned} \tilde{\mathbf{H}}_1^1 &= -\Phi_{r_u}^\top Q(D_x \Phi_{r_u} \otimes \Phi_{r_u}), & \tilde{\mathbf{H}}_1^2 &= -\Phi_{r_v}^\top Q(D_x \Phi_{r_v} \otimes \Phi_{r_u}), \\ \tilde{\mathbf{H}}_2^1 &= -\Phi_{r_h}^\top D_x Q(\Phi_{r_h} \otimes \Phi_{r_u}), & \tilde{\mathbf{H}}_2^2 &= -\Phi_{r_u}^\top Q(\Phi_{r_v} \otimes D_y \Phi_{r_u}), \\ \tilde{\mathbf{H}}_2^3 &= -\Phi_{r_v}^\top Q(\Phi_{r_v} \otimes D_y \Phi_{r_v}), & \tilde{\mathbf{H}}_2^4 &= -\Phi_{r_s}^\top Q(D_x \Phi_{r_s} \otimes \Phi_{r_u}), \\ \tilde{\mathbf{H}}_3^1 &= -\Phi_{r_h}^\top D_y Q(\Phi_{r_h} \otimes \Phi_{r_v}), & \tilde{\mathbf{H}}_3^2 &= -\frac{1}{2} \Phi_{r_u}^\top Q(\Phi_{r_h} \otimes D_x \Phi_{r_s}), \\ \tilde{\mathbf{H}}_3^3 &= -\frac{1}{2} \Phi_{r_v}^\top Q(\Phi_{r_h} \otimes D_y \Phi_{r_s}), & \tilde{\mathbf{H}}_3^4 &= -\Phi_{r_s}^\top Q(D_y \Phi_{r_s} \otimes \Phi_{r_v}), \\ \tilde{\mathbf{H}}_4^1 &= -\Phi_{r_u}^\top Q(\Phi_{r_s} \otimes D_x \Phi_{r_h}), & \tilde{\mathbf{H}}_4^2 &= -\Phi_{r_v}^\top Q(\Phi_{r_s} \otimes D_y \Phi_{r_h}), \end{aligned} \quad (12)$$

where $Q \in \mathbb{R}^{N \times N^2}$ is the matricized tensor such that $Q(\mathbf{a} \otimes \mathbf{b}) = \mathbf{a} \circ \mathbf{b}$ is satisfied for any vectors $\mathbf{a}, \mathbf{b} \in \mathbb{R}^N$.

All the reduced quadratic operators in (12) are computed in the offline stage. In computing reduced quadratic operators, we follow the tensorial approach in [Karasözen et al.(2021)Karasözen, Yıldız, and Uzunca] by exploiting the structure of Kronecker product for computation of the quadratic operators. For instance, consider the computation of the term $\Phi_{r_h}^\top D_x Q(\Phi_{r_h} \otimes \Phi_{r_u})$ which can be computed in MATLAB notation as follows

$$\Phi_{r_h}^\top D_x Q(\Phi_{r_h} \otimes \Phi_{r_u}) = \Phi_{r_h}^\top D_x \begin{pmatrix} \Phi_{r_h}(1, :) \otimes \Phi_{r_u}(1, :) \\ \vdots \\ \Phi_{r_h}(N, :) \otimes \Phi_{r_u}(N, :) \end{pmatrix}. \quad (13)$$

Alternatively, the computation of $G := Q(\Phi_{r_h} \otimes \Phi_{r_u}) \in \mathbb{R}^{N \times r^2}$ can be written as

$$G(i, :) = \left(\text{vec} \left(\Phi_{r_u}^T \Phi_{r_h}(i, :) \right) \right)^T, \quad i = 1, 2, \dots, N,$$

where $\text{vec}(\cdot)$ denotes the vectorization of a matrix. By using "MULTIPROD" [Leva(2008)], the matrix G can efficiently be computed through the calculation of the tensor $\mathcal{G} := \text{MULTIPROD}(\Phi_{r_u}, \hat{\Phi}_{r_h}) \in \mathbb{R}^{N \times r \times r}$, where the tensor $\hat{\Phi}_{r_h} \in \mathbb{R}^{N \times 1 \times r}$ is obtained by reshaping the matrix $\Phi_{r_h} \in \mathbb{R}^{N \times r}$ into $N \times 1 \times r$. Thus, the matrix $G \in \mathbb{R}^{N \times r^2}$ becomes the mode-1 matricization of the tensor \mathcal{G} .

3.2 Operator inference with re-projection

We apply the data-driven, non-intrusive OpInf method [Peherstorfer and Willcox(2016)] with re-projection [Peherstorfer(2020)] to the RTSWE (1). The OpInf projects trajectories of the high-dimensional state spaces of FOMs onto low-dimensional subspaces, and then fit operators to the projected trajectories via least-squares regression. It does not involve any explicit knowledge of the FOM, rather only involves simulation data projected onto the dominant POD subspace. Within OpInf framework, a closure error is introduced into the learned operators, which are different than those of reduced model constructed with the intrusive model reduction. The projected trajectories correspond to non-Markovian dynamics in the low-dimensional subspaces even though the high dimensional full solutions are Markovian [Chorin and Stinis(2006), Givon et al.(2004) Givon, Kupferman, and Stuart]. In Markovian dynamical systems the future states depend only on the current state and not on previous ones, whereas non-Markovian systems can be considered as dynamical systems with a memory so that future states depend on the current and previous states. In [Peherstorfer(2020)], a data sampling scheme is introduced that cancels these non-Markovian dynamics after each time step such that the trajectories correspond to Markovian dynamics in the reduced space. In this way, the OpInf exactly recovers the reduced model from these re-projected trajectories. The data sampling scheme in [Peherstorfer(2020)] iterates between time stepping the high-dimensional FOM and projecting onto low-dimensional reduced subspaces to retain the low-dimensional Markovian dynamics. It was shown in [Peherstorfer(2020)] that under certain conditions, applying OpInf to re-projected trajectories gives the same operators that are obtained with the intrusive model reduction in the limit of $r \rightarrow N$ for many dynamical systems with polynomial nonlinear terms. This is validated in the numerical results in Section (4) so that the learnt low-dimensional models have almost the same level of accuracy as the intrusive reduced models.

Using the definitions from the previous section, the reduced trajectories for each state are denoted as

$$\begin{aligned} \widehat{W}_h(\mu) &= \Phi_{r_h}^\top W_h(\mu) \in \mathbb{R}^{r \times K}, & \widehat{W}_u(\mu) &= \Phi_{r_u}^\top W_u(\mu) \in \mathbb{R}^{r \times K}, \\ \widehat{W}_v(\mu) &= \Phi_{r_v}^\top W_v(\mu) \in \mathbb{R}^{r \times K}, & \widehat{W}_s(\mu) &= \Phi_{r_s}^\top W_s(\mu) \in \mathbb{R}^{r \times K}. \end{aligned}$$

Furthermore, the time derivatives and their projections are given by

$$\begin{aligned} \dot{W}_h(\mu) &= [\dot{\mathbf{h}}^1(\mu), \dots, \dot{\mathbf{h}}^K(\mu)], & \dot{W}_u(\mu) &= [\dot{\mathbf{u}}^1(\mu), \dots, \dot{\mathbf{u}}^K(\mu)], \\ \dot{W}_v(\mu) &= [\dot{\mathbf{v}}^1(\mu), \dots, \dot{\mathbf{v}}^K(\mu)], & \dot{W}_s(\mu) &= [\dot{\mathbf{s}}^1(\mu), \dots, \dot{\mathbf{s}}^K(\mu)], \\ \dot{\widehat{W}}_h(\mu) &= \Phi_{r_h}^\top \dot{W}_h(\mu), & \dot{\widehat{W}}_u(\mu) &= \Phi_{r_u}^\top \dot{W}_u(\mu), \\ \dot{\widehat{W}}_v(\mu) &= \Phi_{r_v}^\top \dot{W}_v(\mu), & \dot{\widehat{W}}_s(\mu) &= \Phi_{r_s}^\top \dot{W}_s(\mu). \end{aligned}$$

We compute the time derivatives by evaluating the right-hand side of the RTSWE (6). Alternatively, the time derivatives can be approximated using finite differences [Martins and Hwang(2013)]. The reduced operators are recovered by solving the following least-squares problems separately for each state vector

$$\min_{\mathcal{X}_j} \sum_{k=1}^M \left\| \mathcal{A}_j(\mu_k) \mathcal{X}_j^\top - \dot{\widehat{W}}_j(\mu_k)^\top \right\|_F^2, \quad j = h, u, v, s, \quad (14)$$

where the data matrices are defined by

$$\begin{aligned} \mathcal{A}_h(\mu_k) &= \left[(\widehat{W}_h(\mu_k) \hat{\otimes} \widehat{W}_u(\mu_k))^\top, (\widehat{W}_h(\mu_k) \hat{\otimes} \widehat{W}_v(\mu_k))^\top \right] \in \mathbb{R}^{K \times 2r^2}, \\ \mathcal{A}_u(\mu_k) &= \left[(\widehat{W}_u(\mu_k) \hat{\otimes} \widehat{W}_u(\mu_k))^\top, (\widehat{W}_v(\mu_k) \hat{\otimes} \widehat{W}_u(\mu_k))^\top, (\widehat{W}_h(\mu_k) \hat{\otimes} \widehat{W}_s(\mu_k))^\top, f(\mu_k) \widehat{W}_v(\mu_k)^\top \right] \in \mathbb{R}^{K \times (3r^2 + r)}, \\ \mathcal{A}_s(\mu_k) &= \left[(\widehat{W}_u(\mu_k) \hat{\otimes} \widehat{W}_s(\mu_k))^\top, (\widehat{W}_v(\mu_k) \hat{\otimes} \widehat{W}_s(\mu_k))^\top \right] \in \mathbb{R}^{K \times 2r^2}, \\ \mathcal{A}_v(\mu_k) &= \left[(\widehat{W}_u(\mu_k) \hat{\otimes} \widehat{W}_v(\mu_k))^\top, (\widehat{W}_v(\mu_k) \hat{\otimes} \widehat{W}_v(\mu_k))^\top, (\widehat{W}_h(\mu_k) \hat{\otimes} \widehat{W}_s(\mu_k))^\top, f(\mu_k) \widehat{W}_u(\mu_k)^\top \right] \in \mathbb{R}^{K \times (3r^2 + r)}, \end{aligned}$$

where $\hat{\otimes}$ stands for the column-wise Kronecker product (Khatri-Rao product), and the learned operators \mathcal{X}_j have the following form

$$\begin{aligned}\mathcal{X}_h &= [\hat{\mathcal{H}}_{1,1}, \hat{\mathcal{H}}_{1,2}] \in \mathbb{R}^{r \times 2r^2}, \quad \mathcal{X}_u = [\hat{\mathcal{H}}_{2,1}, \hat{\mathcal{H}}_{2,2}, \hat{\mathcal{H}}_{2,3}, \hat{\mathcal{L}}_1(\mu)] \in \mathbb{R}^{r \times (3r^2+r)}, \\ \mathcal{X}_s &= [\hat{\mathcal{H}}_{4,1}, \hat{\mathcal{H}}_{4,2}] \in \mathbb{R}^{r \times 2r^2}, \quad \mathcal{X}_v = [\hat{\mathcal{H}}_{3,1}, \hat{\mathcal{H}}_{3,2}, \hat{\mathcal{H}}_{3,3}, \hat{\mathcal{L}}_2(\mu)] \in \mathbb{R}^{r \times (3r^2+r)}.\end{aligned}$$

The least-squares problem (14) can be written in compact form as

$$\min_{\mathcal{X}_j} \left\| \mathcal{A}_{\mu j} \mathcal{X}_j^\top - \hat{W}_{\mu j} \right\|_F^2, \quad j = h, u, v, s, \quad (15)$$

where $\hat{W}_{\mu j} = [\hat{W}_j^T(\mu_1), \dots, \hat{W}_j^T(\mu_M)]^T$ and $\mathcal{A}_{\mu j} = [\mathcal{A}_j^T(\mu_1), \dots, \mathcal{A}_j^T(\mu_M)]^T$ for $j = h, u, v, s$.

We remark that each of the least squares problems (14) are independent and are solved separately to increase the computational efficiency in the online stage [Peherstorfer and Willcox(2016)].

The ROM in the OpInf framework is given as

$$\begin{aligned}\dot{\hat{\mathbf{h}}}(t; \mu) &= \hat{\mathcal{H}}_{1,1}(\hat{\mathbf{h}}(t; \mu) \hat{\otimes} \hat{\mathbf{u}}(t; \mu)) + \hat{\mathcal{H}}_{1,2}(\hat{\mathbf{h}}(t; \mu) \hat{\otimes} \hat{\mathbf{v}}(t; \mu)) \\ \dot{\hat{\mathbf{u}}}(t; \mu) &= \hat{\mathcal{H}}_{2,1}(\hat{\mathbf{u}}(t; \mu) \hat{\otimes} \hat{\mathbf{u}}(t; \mu)) + \hat{\mathcal{H}}_{2,2}(\hat{\mathbf{v}}(t; \mu) \hat{\otimes} \hat{\mathbf{u}}(t; \mu)) + \hat{\mathcal{H}}_{2,3}(\hat{\mathbf{h}}(t; \mu) \hat{\otimes} \hat{\mathbf{s}}(t; \mu)) + f(\mu) \hat{\mathcal{L}}_1 \hat{\mathbf{v}}(t; \mu) \\ \dot{\hat{\mathbf{v}}}(t; \mu) &= \hat{\mathcal{H}}_{3,1}(\hat{\mathbf{u}}(t; \mu) \hat{\otimes} \hat{\mathbf{v}}(t; \mu)) + \hat{\mathcal{H}}_{3,2}(\hat{\mathbf{v}}(t; \mu) \hat{\otimes} \hat{\mathbf{v}}(t; \mu)) + \hat{\mathcal{H}}_{3,3}(\hat{\mathbf{h}}(t; \mu) \hat{\otimes} \hat{\mathbf{s}}(t; \mu)) + f(\mu) \hat{\mathcal{L}}_2 \hat{\mathbf{u}}(t; \mu) \\ \dot{\hat{\mathbf{s}}}(t; \mu) &= \hat{\mathcal{H}}_{4,1}(\hat{\mathbf{u}}(t; \mu) \hat{\otimes} \hat{\mathbf{s}}(t; \mu)) + \hat{\mathcal{H}}_{4,2}(\hat{\mathbf{v}}(t; \mu) \hat{\otimes} \hat{\mathbf{s}}(t; \mu)).\end{aligned}$$

Data sampling via re-projection [Peherstorfer(2020)] is summarized in Algorithm (1) by maintaining the coupling structure of the ROM as in [Qian et al.(2020)Qian, Kramer, Peherstorfer, and Willcox], while the process of the operator inference with re-projection for parametric RTSWE is given in Algorithm (2).

Algorithm 1 Data sampling via re-projection

```

1: procedure RE-PROJECTION
2:   Input: States  $\mathbf{w}^j$   $j = 1, \dots, K$  and POD basis matrix  $\Phi_r$ 
3:   for  $j = 1, \dots, K$  do
4:     Set  $\mathbf{w}_{\text{proj}}^j = (\mathbf{h}_{\text{proj}}^j, \mathbf{u}_{\text{proj}}^j, \mathbf{v}_{\text{proj}}^j, \mathbf{s}_{\text{proj}}^j)^T = \Phi_r \Phi_r^T \mathbf{w}^j$ 
5:     Query FOM at each time step for  $\bar{\mathbf{w}}^j = \Phi_r^T \mathbf{F}(\mathbf{w}_{\text{proj}}^j)$  in (6)
6:     Re-project the states  $\bar{\mathbf{w}}^j = \Phi_r^T \mathbf{w}_{\text{proj}}^j$ 
7:   end for
8:   return  $\bar{\mathbf{W}} = [\bar{\mathbf{w}}^1, \dots, \bar{\mathbf{w}}^K]$  and  $\bar{\mathbf{W}} = [\bar{\mathbf{w}}^1, \dots, \bar{\mathbf{w}}^K]$ 
9: end procedure
    
```

For quadratic systems like the RTSWE, the number of the time steps should satisfy $K \geq r + r^2$, so that the least square system (14) is overdetermined and a unique solution exists according to the Corollary 3.2 in [Peherstorfer(2020)] and the data matrices \mathcal{A}_j , $j = h, u, v, s$ have full rank. When this condition is not fulfilled, the least-squares problem (15) is underdetermined and therefore uniqueness of the solution is lost. The least-squares problem arising in OpInf can be ill-conditioned; thus, regularization should be applied. The common regularization techniques are the truncated SVD and the Tikhonov regularization [Tikhonov and Arsenin(1977)]. An ill-conditioned matrix as either a matrix with a well-determined numerical rank or an ill-determined numerical rank, depending on the behavior of the singular value spectrum [Hansen(1987)]. Usually, the L-curve criterion [Hansen(2000)] is used to determine the tolerance at which the singular values are truncated. Analyzing the L-curve, a tolerance can be determined that has a good compromise between the matching of data-fidelity term and making the problem well-conditioned. As it will be illustrated in Section 4, the singular values of the data matrices decay monotonically without exhibiting a gap. According to terminology in [Hansen(1987)], the numerical rank of the data matrices is ill-determined. The L-curve also does not provide any information; there exist not an optimal value for the tolerance, consequently truncated SVD can not be used. One way to overcome this bottleneck is to solve the least-squares problem via the minimum norm of the solution. The minimum-norm solution enforces uniqueness of the solution by picking smallest $\|\mathcal{X}_j\|_F$ which minimizes $\|\mathcal{A}_{\mu j} \mathcal{X}_j^\top - \hat{W}_{\mu j}\|_F$. To obtain the minimum-norm solution, one can use the Moore-Penrose pseudoinverse

Algorithm 2 Operator inference with re-projection for parametric RTSWE

-
- 1: **procedure** OPINF
 - 2: **Input:** States $\mathbf{w}_j(\mu_i)$ and time derivatives $\dot{\mathbf{w}}_j(\mu_i)$ for $i = 1, \dots, M$ and $j = 1, \dots, K$
 - 3: Construct the trajectories for each state

$$W_h(\mu) = [\mathbf{h}_1(\mu), \dots, \mathbf{h}_K(\mu)], \quad W_u(\mu) = [\mathbf{u}_1(\mu), \dots, \mathbf{u}_K(\mu)],$$

$$W_v(\mu) = [\mathbf{v}_1(\mu), \dots, \mathbf{v}_K(\mu)], \quad W_s(\mu) = [\mathbf{s}_1(\mu), \dots, \mathbf{s}_K(\mu)].$$
 - 4: Construct the global snapshot matrices $W_{j\mu} = [W_j(\mu_1), \dots, W_j(\mu_M)]$ for $j = h, u, v, s$
 - 5: Compute the global POD basis Φ_{rj} of $W_{j\mu}$ for $j = h, u, v, s$
 - 6: Sample the data via re-projection and set $\widehat{W}_j = \overline{W}_j$ and $\widehat{\dot{W}}_j = \dot{\overline{W}}_j$ for $j = h, u, v, s$
 - 7: Determine the tolerance of `lsqminnorm` tol , using L-curve formula
 - 8: Solve the least-squares problem (14) to obtain operators of the reduced-order system using

$$\mathcal{X}_j^T = \text{lsqminnorm}(\mathcal{A}_{\mu j}, \widehat{W}_{\mu j}, tol)$$
 - 9: **end procedure**
-

or complete orthogonal decomposition (COD) formulas. We use here MATLAB's routine `lsqminnorm` as regularizer of the least-squares problem (14) to achieve the uniqueness. The tolerance will be determined with the L-curve as shown in Section 4.

Under the conditions that the time stepping scheme for the FOM is convergent as $\Delta t \rightarrow 0$, the derivatives approximated from the projected states $\hat{\mathbf{w}}$ converge to $\frac{d}{dt}\hat{\mathbf{w}}(t_k)$ as $\Delta t \rightarrow 0$, and the data matrix is of full rank, then the learned operators \hat{A}, \hat{H} converge to the intrusively projected operators \tilde{A}, \tilde{H} [Qian et al.(2020)Qian, Kramer, Peherstorfer, and Willcox, Peherstorfer and Willcox(2016)]. Kahan's method is second order convergent, the data matrix is of full rank, therefore these conditions above are fulfilled.

In the OpInf framework, once the operators are inferred, any time stepping scheme can be used to solve the ROM with the inferred operators, because the operators of the system of ODEs are inferred and not the operators of the time-discretized system. Here, we use again Kahan's method as time-discretization scheme for (7), because it is cheap, i.e., linearly implicit, and preserves the conserved quantities in contrast to the implicit or explicit Euler methods.

3.3 Computational aspects

The costs of the data generation and the construction of the POD basis are the same for the POD-G and the OpInf. We, therefore, consider the costs of the OpInf Algorithm (2) and compare it to the cost of the intrusive MOR in Section (3.1).

The computational cost of the OpInf Algorithm (2) is dominated by querying the high-dimensional system. The costs of the projection of the trajectories onto the POD space are of order $\mathcal{O}(rNK)$ and thus are bounded linearly in the dimension N of the FOM and the number of time steps K for each parameter value μ_k . The data matrices \mathcal{A}_j , $j = h, u, v, s$ and the right-hand side matrices \widehat{W}_j , $j = h, u, v, s$ are assembled with the costs at most $\mathcal{O}(MK(3r^2 + r))$ and $\mathcal{O}(MKr)$, respectively. The leading costs of solving one of the r independent least-squares problems for each state vector h, u, v, s is $\mathcal{O}(KM^6r^6)$, see, e.g., [Peherstorfer and Willcox(2016)]. Overall, the cost of Algorithm (2) is bounded linearly in the dimension N of the FOM and linearly in the number of time steps K . Only the projection of the trajectories onto the POD space incurs cost that scale with the dimension N of the FOM. All other computations in Algorithm (2) have cost independent of the dimension N of the FOM. Additional cost occurs in generating the re-projected trajectories and the time derivatives, which depends on the number of time steps K used for generating the re-projected trajectories. Therefore, the computational cost of OpInf Algorithm (2) with re-projection is twice of OpInf without re-projection.

A data matrix with a large condition number can introduce significant numerical errors into the solutions of the r least-squares problems, and thus into the inferred operators. Increasing the dimension r of the reduced space decreases the ROM error, but increases the degrees of freedom in OpInf, so that the data matrix becomes ill-conditioned. A large condition number typically arises if the states at different time steps are almost linearly dependent in the case of parametric systems. There exist several heuristic strategies that might help to reduce the condition number of the data matrix. The condition number of the least-squares problem can be decreased by sampling in a subset of trajectories as well as the computational efficiency can be increased, by taking every k -th snapshot in the data matrix [Peherstorfer and Willcox(2016)]. The condition number decreases adding more training data, starting to solve the

FOM with different initial values [Peherstorfer and Willcox(2016)] because the first r POD basis becomes richer [Swischuk et al.(2019)Swischuk, Mainini, Peherstorfer, and Willcox]. Both strategies are employed in Section 4.

4 Numerical results

In this section, we compare the accuracy, computational efficiency and the prediction capabilities of the POD-G and OpInf in the parametric and in the non-parametric form for the double vortex RTSWE [Eldred et al.(2019)Eldred, Dubos, and Kritsikis] in a doubly periodic domain $\Omega = [0, L]^2$ without the bottom topography ($b = 0$). The initial conditions are given by

$$\begin{aligned} h_0(x, y) &= H_0 - \Delta h \left[e^{-0.5((x'_1)^2 + (y'_1)^2)} + e^{-0.5((x'_2)^2 + (y'_2)^2)} - \frac{4\pi\sigma_x\sigma_y}{L^2} \right], \\ u_0(x, y) &= \frac{-g\Delta h}{f\sigma_y} \left[y_1'' e^{-0.5((x'_1)^2 + (y'_1)^2)} + y_2'' e^{-0.5((x'_2)^2 + (y'_2)^2)} \right], \\ v_0(x, y) &= \frac{g\Delta h}{f\sigma_x} \left[x_1'' e^{-0.5((x'_1)^2 + (y'_1)^2)} + x_2'' e^{-0.5((x'_2)^2 + (y'_2)^2)} \right], \\ s_0(x, y) &= g \left(1 + 0.05 \sin \left[\frac{2\pi}{L}(x - xc) \right] \right), \end{aligned}$$

where $xc = 0.5L$ and

$$\begin{aligned} x'_1 &= \frac{L}{\pi\sigma_x} \sin \left[\frac{\pi}{L}(x - xc_1) \right], & x'_2 &= \frac{L}{\pi\sigma_x} \sin \left[\frac{\pi}{L}(x - xc_2) \right], \\ y'_1 &= \frac{L}{\pi\sigma_y} \sin \left[\frac{\pi}{L}(y - yc_1) \right], & y'_2 &= \frac{L}{\pi\sigma_y} \sin \left[\frac{\pi}{L}(y - yc_2) \right] \\ x''_1 &= \frac{L}{2\pi\sigma_x} \sin \left[\frac{2\pi}{L}(x - xc_1) \right], & x''_2 &= \frac{L}{2\pi\sigma_x} \sin \left[\frac{2\pi}{L}(x - xc_2) \right], \\ y''_1 &= \frac{L}{2\pi\sigma_y} \sin \left[\frac{2\pi}{L}(y - yc_1) \right], & y''_2 &= \frac{L}{2\pi\sigma_y} \sin \left[\frac{2\pi}{L}(y - yc_2) \right]. \end{aligned}$$

The center of the two vortices are given by

$$xc_1 = (0.5 - ox)L, \quad xc_2 = (0.5 + ox)L, \quad yc_1 = (0.5 - oy)L, \quad yc_2 = (0.5 + oy)L.$$

We set parameter values $L = 5000\text{km}$, $H_0 = 750\text{m}$, $h = 75\text{m}$, $g = 9.80616\text{ms}^{-2}$, $\sigma_x = \sigma_y = 3L/40$ and $ox = oy = 0.1$. All simulations are performed on a grid with the mesh sizes $n_x = n_y = 120\text{km}$ on a machine with Intel® Core™ i7 2.5 GHz 64 bit CPU, 8 GB RAM, Windows 10, using 64 bit MatLab R2019a.

4.1 The non-parametric case

For the non-parametric case, we take Coriolis parameter as $f = 0.00006147\text{s}^{-1}$ at the latitude 7, close to equator and the number of time steps are set to $K = 250$ with the time step-size $\Delta t = 486\text{s}$, that leads to the final time $T = 33\text{h } 45\text{min}$ [Eldred et al.(2019)Eldred, Dubos, and Kritsikis]. The size of each snapshot matrix of the FOM is 14440×250 .

The accuracy of the ROMs is measured using the relative error of the four states

$$\frac{\|\Phi_r Z - W\|_F}{\|W\|_F}, \quad (16)$$

where $W \in \mathbb{R}^{4N \times K}$ is the snapshot matrix of the FOM and $Z \in \mathbb{R}^{4r \times K}$ is the snapshot matrix of either the non-intrusive or the intrusive ROMs. The average relative errors between FOM and ROM solutions are given for each state variable $\mathbf{w} = \mathbf{u}, \mathbf{v}, \mathbf{h}, \mathbf{s}$ in the time-averaged $L^2(\Omega)$ -norms as

$$\|\mathbf{w} - \mathbf{w}_r\|_{rel} = \frac{1}{K} \sum_{k=1}^{N_t} \frac{\|\mathbf{w}^k - \mathbf{w}_r^k\|_{L^2}}{\|\mathbf{w}^k\|_{L^2}}, \quad \|\mathbf{w}^k\|_{L^2}^2 = \sum_{i=1}^n \sum_{j=1}^n (w_{i,j}^k)^2 \Delta x \Delta y, \quad (17)$$

where \mathbf{w}_r denotes the reduced approximation to the full solution \mathbf{w} , either of the G-POD $\hat{\mathbf{w}}$ or OpInf $\tilde{\mathbf{w}}$.

Conservation of the discrete conserved quantities (8): the energy, mass, buoyancy, and total vorticity obtained by the FOM and ROM solutions are measured using the time-averaged relative error defined by

$$\frac{1}{K} \sum_{k=1}^K \frac{|E(\mathbf{w}^k) - E(\mathbf{w}^0)|}{|E(\mathbf{w}^0)|}, \quad E \equiv H, M, B, Q. \quad (18)$$

Firstly, we illustrate how the tolerance tol in Algorithm 2 is determined for the regularization of the least-squares problem (15). Singular values of the data matrices in Figure 1 decay without exhibiting a gap. Therefore, the L-curve does not provide any information to determine the tolerances for the truncated SVD.

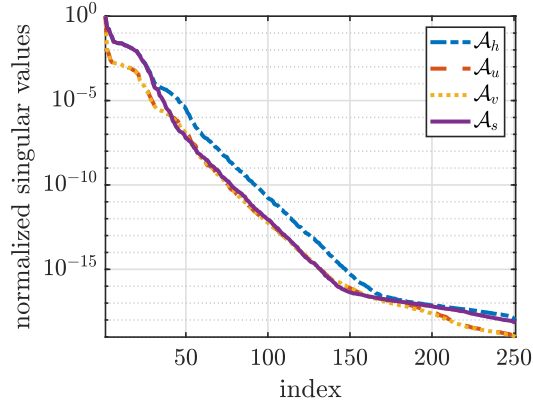
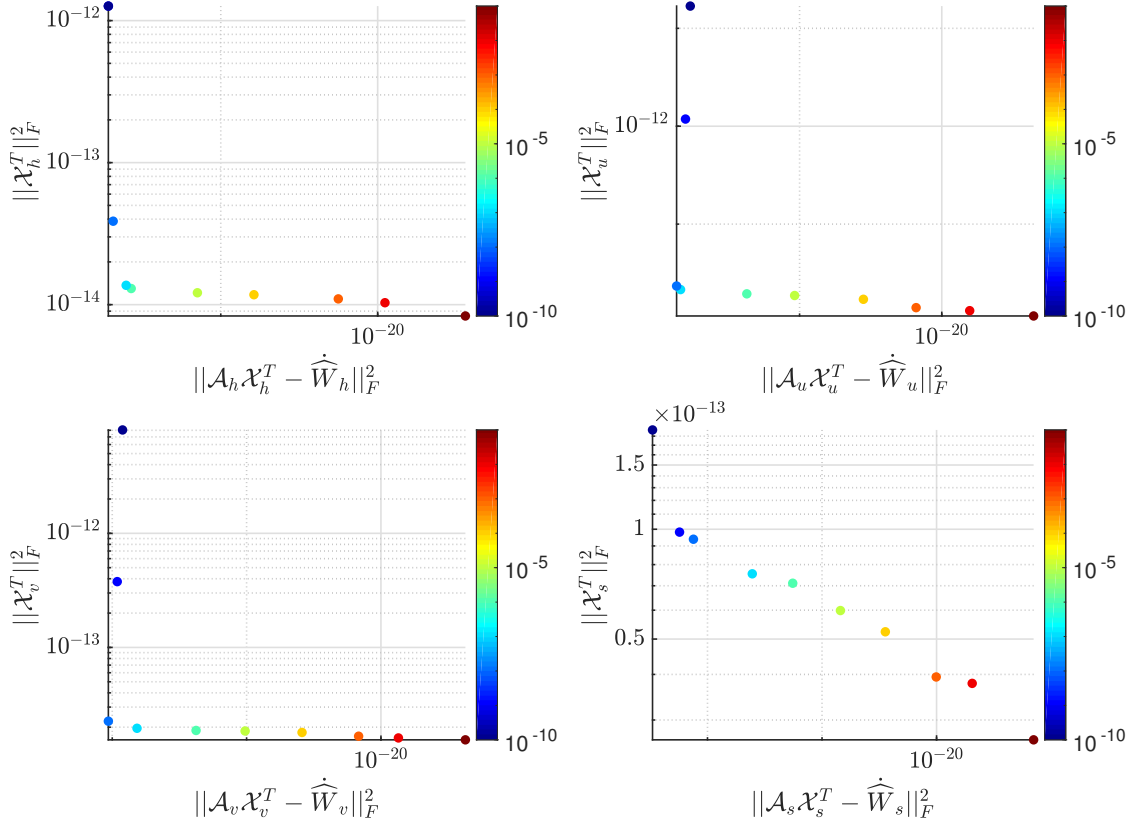


Figure 1: Normalized singular values of the data matrices for the reduced dimension $r = 20$.

The tolerances of the least-squares minimum norm solver routine `lsqminnorm` are determined by the L-curves of the data matrices in Figure 2 as $1e-6$ for $j = h, v$ and $1e-7$ for $j = u, s$.

Figure 2: L-curves for reduced dimension $r = 20$.

In Figure 3, the singular values decay relatively slowly, as for the complex fluid dynamic problems with wave and transport phenomena like the SWEs [Ohlberger and Rave(2016)].

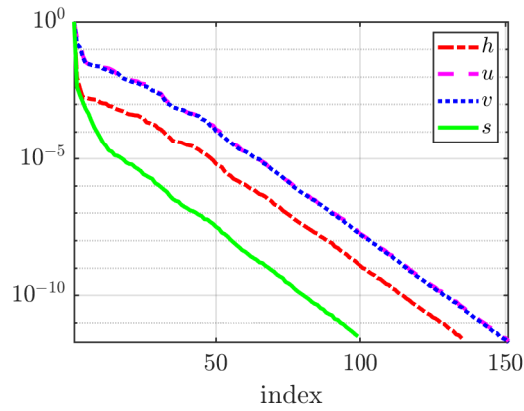


Figure 3: Normalized singular values of the snapshot matrices.

In Figure 4, the relative FOM-ROM errors (16) of the four states are plotted. The errors of the POD-G and OpInf are very close. With increasing reduced dimension r , the POD-G and OpInf errors decrease. Average relative errors (17) of the POD-G and OpInf are $1.499e-03$ and $1.485e-03$, relatively, for the reduced dimension $r = 20$, which shows that both ROMs approximate the FOM with the same level of accuracy.

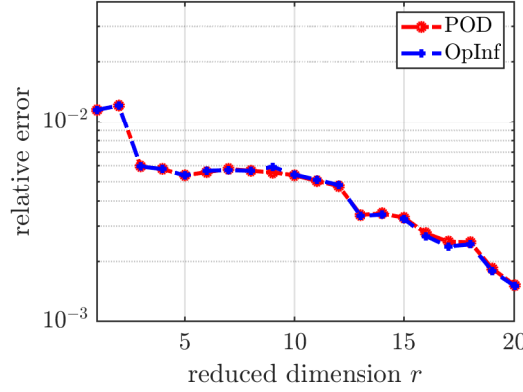


Figure 4: Relative errors (16) of the POD-G and OpInf.

Next, we show the total computational times for the POD-G and OpInf algorithms in Figure 5, where we exclude the computation time of obtaining POD basis since it is common for the POD-G and OpInf algorithms. The computational time consists of the time for constructing the reduced tensors (12) and online computation time for the POD-G algorithm, whereas in the OpInf algorithm it consists of the elapsed time of constructing the re-projected states and time derivatives, solving the least-squares problem (14), and online computation time. The computational cost of the OpInf is larger than the POD-G due to re-projection. The total computational times in Figure 5 are 1.044s for the POD-G, and 2.045s for OpInf, both of which show a speedup of order 10^2 over the FOM with 585.129s computing time.

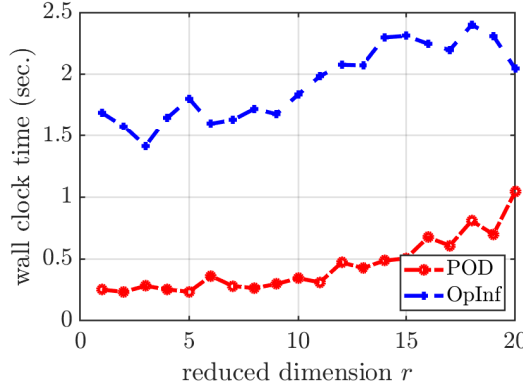


Figure 5: Elapsed total computational time of the ROMs.

Both ROMs reproduce the full solutions accurately at the final time in Figure 6 for the reduced dimension $r = 20$. In Figure 7, the relative errors in the Hamiltonian (energy) $|H^k - H^0|/|H^0|$, mass $|M^k - M^0|/|M^0|$, buoyancy $|B^k - B^0|/|B^0|$, and the total potential vorticity $|Q^k - Q^0|/|Q^0|$ are plotted over the time steps. The total mass and the total potential vorticity are preserved up to machine precision. The energy and buoyancy errors of both ROMs show bounded oscillations over time without any drift, i.e., they are preserved well in long-term. Preservation of conserved quantities by the ROMs is shown in Table 1 in terms of the relative errors (18).

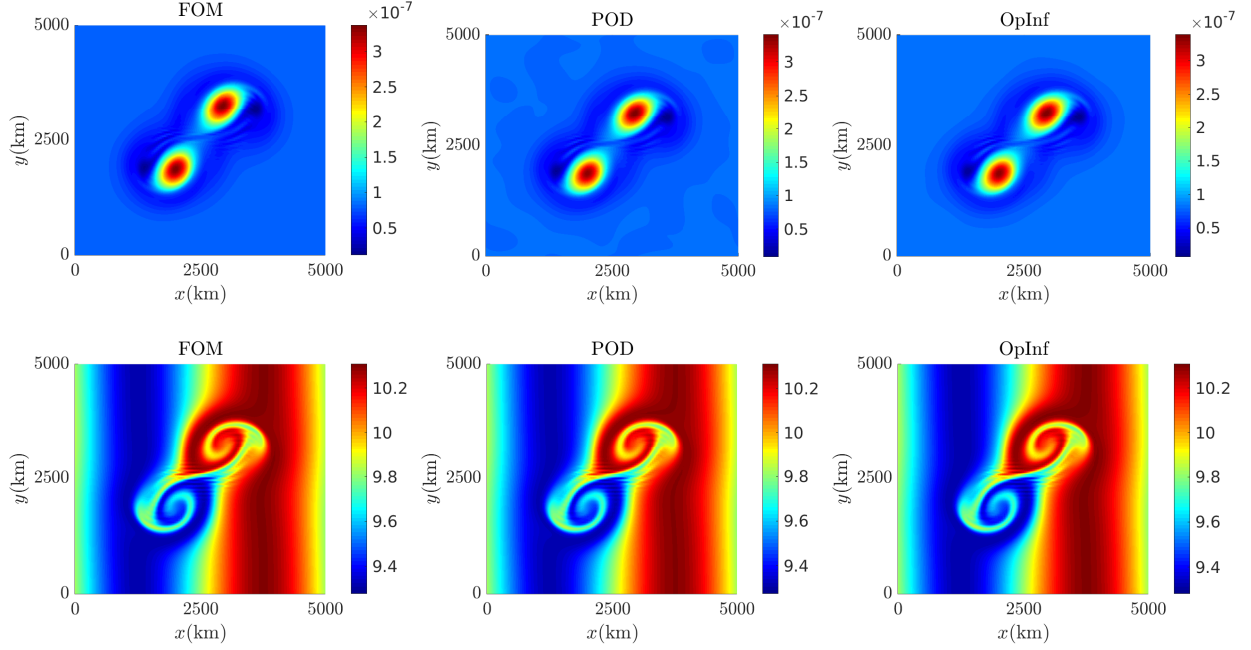


Figure 6: (Top) Vorticity and (bottom) buoyancy of the FOM and ROMs at the final time.

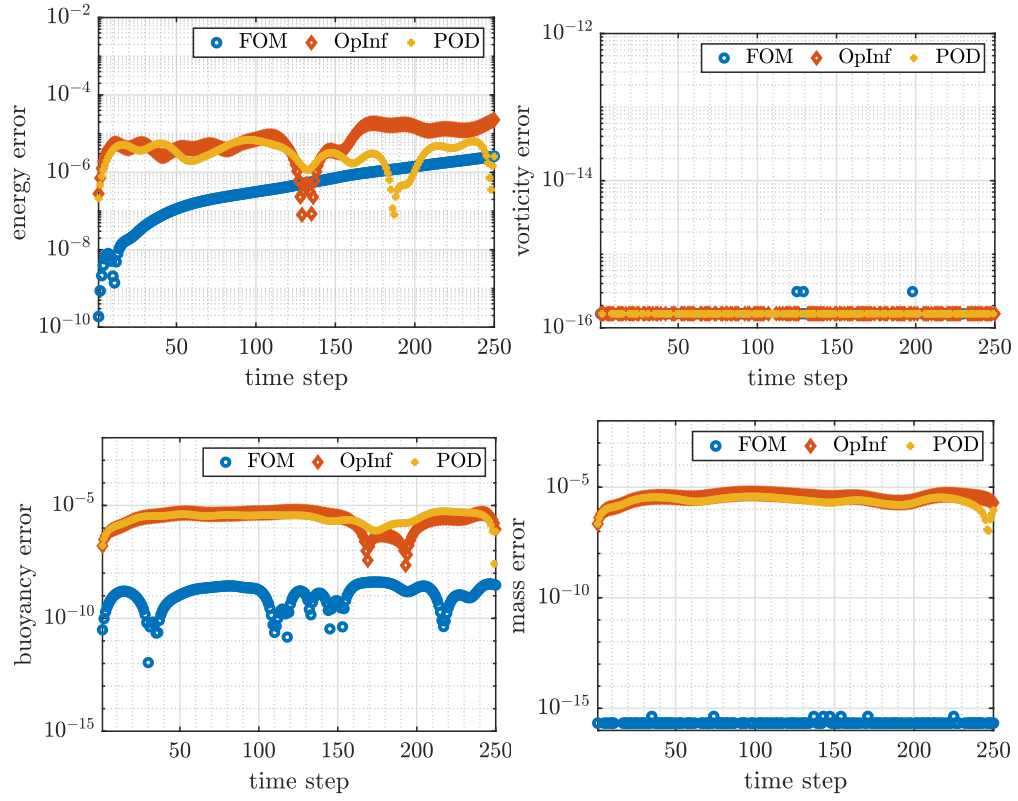


Figure 7: Relative errors in the conserved quantities.

Table 1: Time-averaged relative errors (18) of the conserved quantities.

	Energy	Total Vorticity	Mass	Buoyancy
FOM	7.484e-07	6.392e-17	1.545e-16	1.567e-09
POD	3.489e-06	1.024e-16	2.489e-06	3.053e-06
OpInf	8.114e-06	1.018e-16	3.440e-06	3.050e-06

Prediction of the future dynamics of complex systems are investigated with the intrusive and non-intrusive ROMs for the single-injector combustor [McQuarrie et al.(2021)McQuarrie, Huang, and Willcox], the SWE [Ahmed et al.(2020)Ahmed, San, Bistriani, and Navon], and the quasi-geostrophic equations [Mou et al.(2020)Mou, Liu, Wells, and Iliescu]. Here, we demonstrate the predictive capabilities of both ROM approaches for the RTSWE. For the state vector $\mathbf{w} = (\mathbf{u}, \mathbf{v}, \mathbf{h}, \mathbf{s})$, the relative FOM-ROM error at the time step k is defined as

$$\frac{\|\mathbf{w}^k - \mathbf{w}_r^k\|_{L^2}}{\|\mathbf{w}^k\|_{L^2}}. \quad (19)$$

In Figures 8-9, the relative errors (19) for the state variables are plotted, where the vertical blue lines separate the training and the prediction periods. The training period $[t_0, t_{k-1}]$ is taken of the full time domain $[t_0, t_f]$ for prediction of the dynamics of the buoyancy and the vorticity over the whole time domain $[t_k, t_f]$. We study two cases; shorter and longer training regimes than the prediction regimes in Figures 8 and 9. When the amount of training data gets larger than the prediction period, the ROM predictions improve in Figure 9. Increasing the number of the modes does not affect the ROM predictions significantly in Figures 8-9. In each case, the ROMs are able to accurately re-predict the training data and capture much of the overall system behavior in the prediction phase. Both POD-G and OpInf are able to accurately re-predict the training data and capture much of the overall behavior of the FOMs in the prediction period. An overview of the performance of ROMs in terms of the averaged relative errors (17) is given in Table (2).

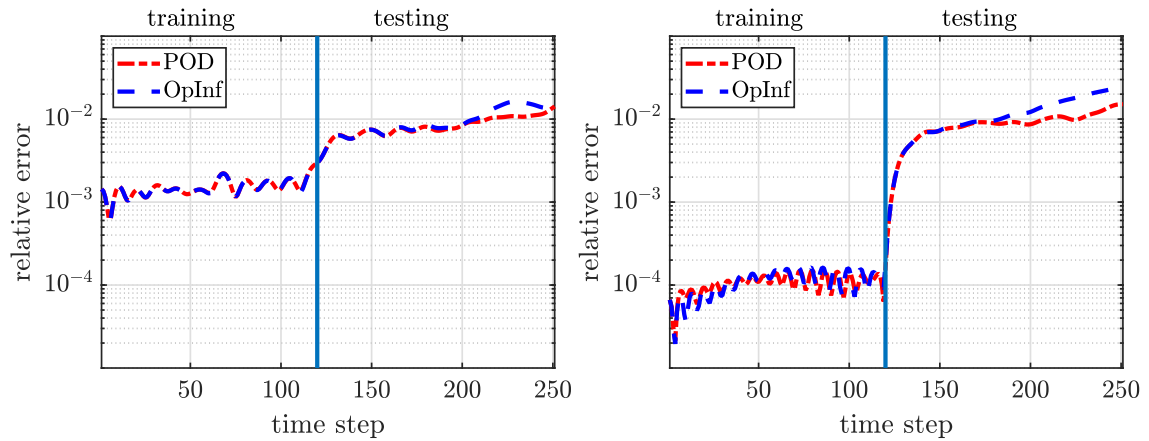


Figure 8: Prediction performance of the ROMs trained up to $K = 120$ with the reduced dimension (left) $r = 10$ and (right) $r = 20$.

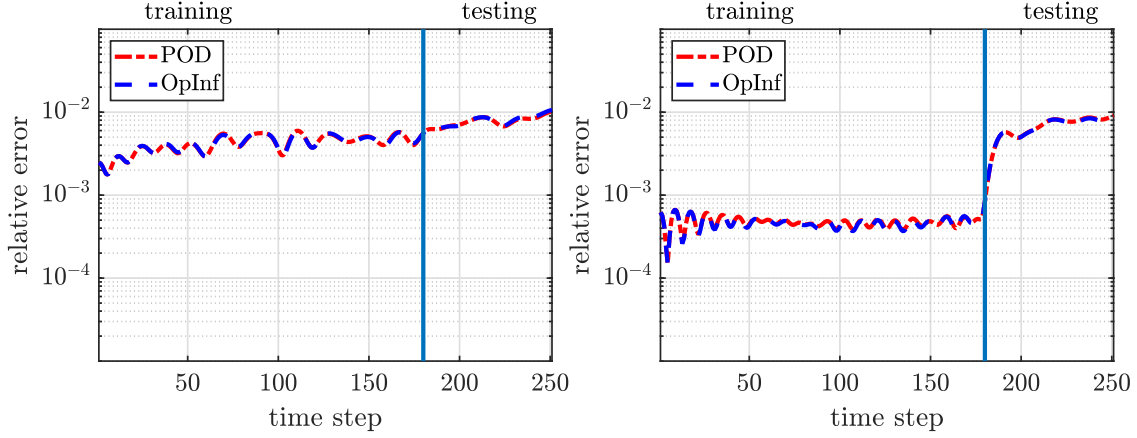


Figure 9: Prediction performance of the ROMs trained up to $K = 120$ with the reduced dimension (left) $r = 10$ and (right) $r = 20$.

Table 2: Average relative errors (17) for training and prediction sets.

		$r = 10$		$r = 20$	
		POD	OpInf	POD	OpInf
$K = 120$	training	1.529e-03	1.523e-03	1.060e-04	1.106e-04
	prediction	8.299e-03	9.487e-03	8.769e-03	1.193e-02
$K = 180$	training	4.250e-03	4.233e-03	4.737e-04	4.637e-04
	prediction	7.691e-03	7.817e-03	6.695e-03	6.587e-03

4.2 The parametric case

For the parametric case, we consider the Coriolis parameter $f(\mu) = 2\Omega \sin(\mu)$ varying with the latitude μ in the parameter domain $\mathcal{D} := 4\pi/18 \leq \mu \leq 8\pi/18$, i.e., between the 40th to 80th latitude. We take a larger time horizon, with the number of time steps $K = 300$, than the one in the non-parametric case in order to reflect the parametric variability of the reduced solutions and to improve the condition number of the data matrices. The average relative errors in the training phase are computed as

$$\frac{1}{M_{train}} \sum_{i=1}^{M_{train}} \frac{\|\Phi_r Z(\mu_i^{train}) - W(\mu_i^{train})\|_F}{\|W(\mu_i^{train})\|_F}, \quad (20)$$

where $W(\mu_i^{train})$ is the FOM trajectory and $Z(\mu_i^{train})$ is the trajectory of either the intrusive reduced model (POD-G) or learned model (OpInf) from the re-projected trajectories. Similarly, the accuracy of the parametric model for the test case is measured via the average relative error defined by

$$\frac{1}{M_{test}} \sum_{i=1}^{M_{test}} \frac{\|\Phi_r Z(\mu_i^{test}) - W(\mu_i^{test})\|_F}{\|W(\mu_i^{test})\|_F}. \quad (21)$$

In the training phase, the intrusive and non-intrusive ROMs are constructed with $M_{train} = 6$ equidistant parameters $\mu_1^{train}, \dots, \mu_{M_{train}}^{train} \in \mathcal{D}$ in the parameter domain \mathcal{D} . Moreover, in order to reduce the condition number of data matrices, we take initial conditions that are randomly perturbed at the center of the vortices as $oy = 0.1 + \gamma$, where γ is a uniformly distributed random value. They do not necessarily have a physical meaning, they reflect the behavior of the FOM over many different initial conditions with the aim to provide more complete information about the FOM and reduce the condition number of the data matrices in the OpInf. The least-squares problem (14) is solved with `lsqminnorm` algorithm with the tolerance $tol = 1e - 10$, and by considering subset of the snapshots, i.e., every 2nd snapshot.

In the testing phase we take $M_{test} = 7$ randomly distributed parameters $\mu_1^{test}, \dots, \mu_{M_{test}}^{test} \in \mathcal{D}$ that are different from the parameters in the training phase. In Figure 10, we demonstrate the relative errors (20) and (21) for the training and testing periods, respectively, over the increasing number of reduced dimension r , which shows that both intrusive

and non-intrusive ROMs behave similarly, resulting more accurate reduced solutions with the increasing number of modes. Figure 11 show that the potential vorticity and buoyancy computed at final time for reduced dimension $r = 10$ with the Coriolis parameter with μ_1^{test} , are resolved accurately with the intrusive and non-intrusive ROMs.

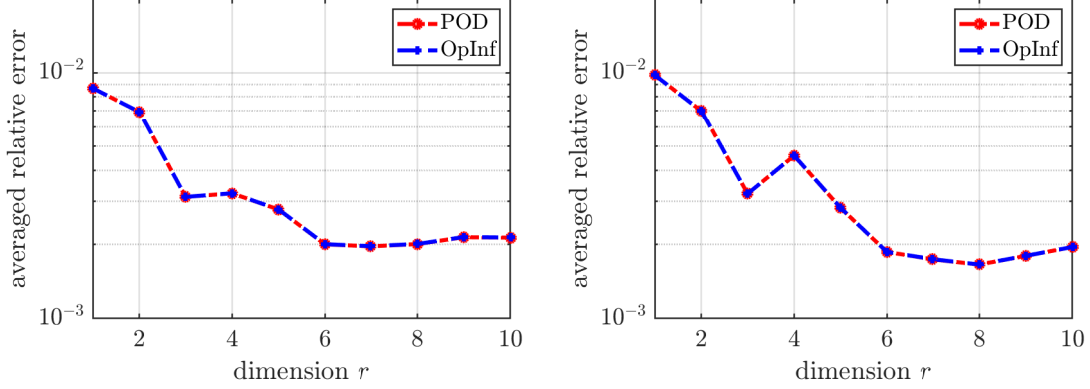


Figure 10: (Left) The relative error (20) in the training period, (right) the relative error (21) in the testing period.

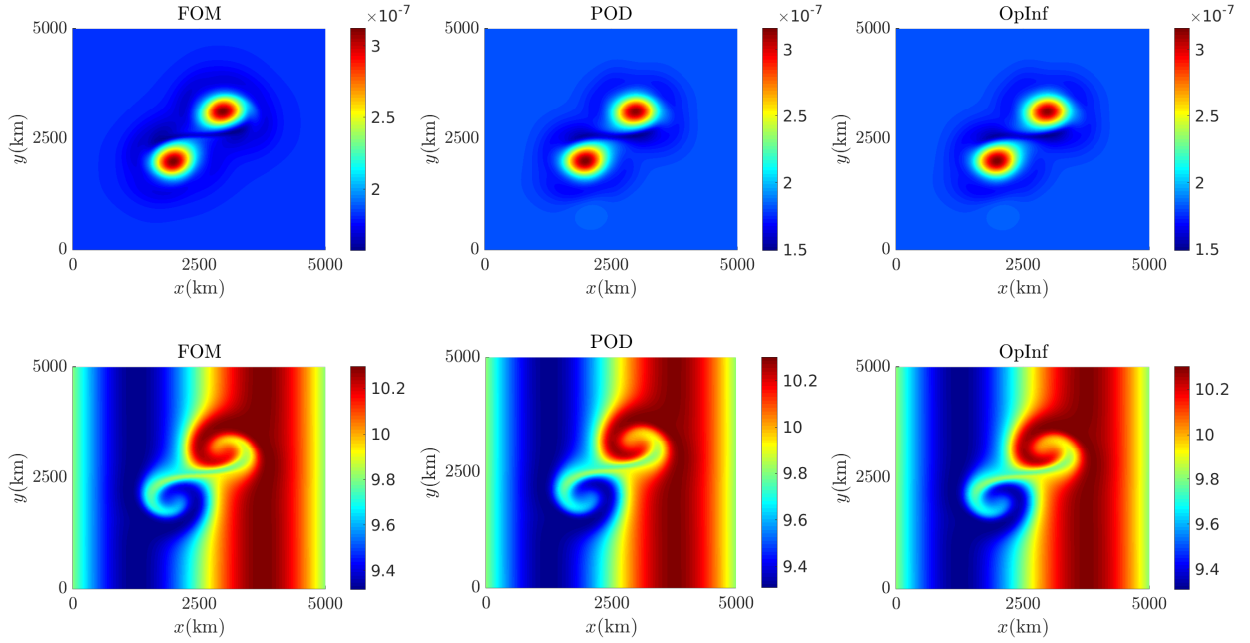


Figure 11: (Top) Vorticity and (bottom) buoyancy of the FOM and ROMs at the final time.

5 Conclusions

In this paper, we have compared the intrusive POG-G with the data-driven non-intrusive OpInf for a complex fluid dynamics model, i.e., RTSWE. Spatial discretization of the RTSWE results in a linear-quadratic system in the Hamiltonian form, which is integrated in time with the energy preserving linearly implicit Kahan's method. In this way, the Hamiltonian structure and the associated invariants of the RTSWE are maintained by the FOM. Numerical results in the parametric and non-parametric settings show that both ROMs behave similarly and yield ROMs that are equal up to numerical errors. This validates the convergence of the learned operators to the intrusively obtained reduced operators under certain conditions on the time discretization in [Peherstorfer and Willcox(2016), Peherstorfer(2020)].

The least-squares problem is regularized with the minimum norm solution which was not used in the operator inference context. Both reduced models are able to accurately re-predict the training data and capture much of the overall system behavior in the prediction period. Due to re-projection, the OpInf is more costly than the POD-G, nevertheless, speed-up factors of order two are achieved by both ROMs. Moreover, preservation of the conserved quantities by both ROMs indicates the stability of the reduced solutions in long-time integration, which is important for Hamiltonian PDEs like the RTSWE. It also indicates the importance of respecting the physics of the complex problems in ROM application.

Both intrusive and non-intrusive techniques can be compared with machine learning techniques. As a future work, we plan to investigate the reduced models of the SWEs with the Hamiltonian neural networks [Jin et al.(2020)Jin, Zhang, Zhu, Tang, and Karniadakis].

Acknowledgements This work was supported by 100/2000 Ph.D. Scholarship Program of the Turkish Higher Education Council.

References

- [Salmon(2004)] R. Salmon. Poisson-bracket approach to the construction of energy- and potential-enstrophy-conserving algorithms for the shallow-water equations. *Journal of the Atmospheric Sciences*, 61(16):2016–2036, 2004. doi:10.1175/1520-0469(2004)061<2016:PATTCO>2.0.CO;2.
- [Dellar(2003)] Paul J. Dellar. Common Hamiltonian structure of the shallow water equations with horizontal temperature gradients and magnetic fields. *Physics of Fluids*, 15(2):292–297, 2003. doi:10.1063/1.1530576.
- [Warneford and Dellar(2013)] Emma S. Warneford and Paul J. Dellar. The quasi-geostrophic theory of the thermal shallow water equations. *Journal of Fluid Mechanics*, 723:374–403, 2013. doi:10.1017/jfm.2013.101.
- [Eldred et al.(2019)Eldred, Dubos, and Kritsikis] Christopher Eldred, Thomas Dubos, and Evaggelos Kritsikis. A quasi-Hamiltonian discretization of the thermal shallow water equations. *Journal of Computational Physics*, 379:1 – 31, 2019. doi:10.1016/j.jcp.2018.10.038.
- [Ripa(1995)] P. Ripa. On improving a one-layer ocean model with thermodynamics. *Journal of Fluid Mechanics*, 303:169–201, 1995. doi:10.1017/S0022112095004228.
- [Zerroukat and Allen(2015)] M. Zerroukat and T. Allen. A moist Boussinesq shallow water equations set for testing atmospheric models. *Journal of Computational Physics*, 290:55 – 72, 2015. ISSN 0021-9991. doi:https://doi.org/10.1016/j.jcp.2015.02.011.
- [Warneford and Dellar(2014)] Emma S. Warneford and Paul J. Dellar. Thermal shallow water models of geostrophic turbulence in Jovian atmospheres. *Physics of Fluids*, 26(1):016603, 2014. doi:10.1063/1.4861123.
- [Dempsey and Rotunno(1988)] David P. Dempsey and Richard Rotunno. Topographic generation of mesoscale vortices in mixed-layer models. *Journal of the Atmospheric Sciences*, 45(20):2961–2978, 1988. doi:10.1175/1520-0469(1988)045<2961:TGOMVI>2.0.CO;2.
- [Young and Chen(1995)] W. R. Young and Lianggui Chen. Baroclinic instability and thermohaline gradient alignment in the mixed layer. *Journal of Physical Oceanography*, 25(12):3172–3185, 12 1995. doi:10.1175/1520-0485(1995)025<3172:BIATGA>2.0.CO;2.
- [Gouzien et al.(2017)Gouzien, Lahaye, Zeitlin, and Dubos] E. Gouzien, N. Lahaye, V. Zeitlin, and T. Dubos. Thermal instability in rotating shallow water with horizontal temperature/density gradients. *Physics of Fluids*, 29(10):101702, 2017. doi:10.1063/1.4996981.
- [Berkooz et al.(1993)Berkooz, Holmes, and Lumley] G Berkooz, P Holmes, and J L Lumley. The proper orthogonal decomposition in the analysis of turbulent flows. *Annual Review of Fluid Mechanics*, 25(1):539–575, 1993. doi:10.1146/annurev.fl.25.010193.002543.
- [Sirovich(1987)] Lawrence Sirovich. Turbulence and the dynamics of coherent structures. III. Dynamics and scaling. *Quart. Appl. Math.*, 45(3):583–590, 1987. doi:10.1090/qam/910464.
- [Barrault et al.(2004)Barrault, Maday, Nguyen, and Patera] Maxime Barrault, Yvon Maday, Ngoc Cuong Nguyen, and Anthony T. Patera. An empirical interpolation method: application to efficient reduced-basis discretization of partial differential equations. *Comptes Rendus Mathématique*, 339(9):667–672, 2004. doi:10.1016/j.crma.2004.08.006.
- [Chaturantabut and Sorensen(2010)] Saifon Chaturantabut and Danny C. Sorensen. Nonlinear model reduction via discrete empirical interpolation. *SIAM J. Sci. Comput.*, 32(5):2737–2764, 2010. doi:10.1137/090766498.

- [Benner et al.(2017)Benner, Cohen, Ohlberger, and Willcox] Peter Benner, Albert Cohen, Mario Ohlberger, and Karen Willcox, editors. *Model Reduction and Approximation*, volume 15 of *Computational Science & Engineering*. Society for Industrial and Applied Mathematics (SIAM), Philadelphia, PA, 2017. doi:10.1137/1.9781611974829.
- [Quarteroni and Rozza(2014)] Alfio Quarteroni and Gianluigi Rozza. *Reduced Order Methods for Modeling and Computational Reduction*, volume 9 of *MS&A*. Springer, Milano, 1 edition, 2014. doi:10.1007/978-3-319-02090-7.
- [Schilders et al.(2021)Schilders, Grivet-Talocia, Benner, Quarteroni, Rozza, and Silveira] Wil Schilders, Stefano Grivet-Talocia, Peter Benner, Alfio Quarteroni, Gianluigi Rozza, and Luís Miguel Silveira. *Snapshot-Based Methods and Algorithms*. De Gruyter, 2021. doi:10.1515/9783110671490.
- [Gibson et al.(2019)Gibson, McRae, Cotter, Mitchell, and Ham] Thomas H. Gibson, Andrew T. T. McRae, Colin J. Cotter, Lawrence Mitchell, and David A. Ham. *Compatible finite element methods for geophysical flows*. SpringerBriefs in Mathematics of Planet Earth. Springer, Cham, 2019. doi:10.1007/978-3-030-23957-2.
- [Delestre et al.(2017)Delestre, Darboux, James, Lucas, Laguerre, and Cordier] Olivier Delestre, Frédéric Darboux, François James, Carine Lucas, Christian Laguerre, and Stéphane Cordier. FullSWOF: Full shallow-water equations for overland flow. *Journal of Open Source Software*, 2(20):448, 2017. doi:10.21105/joss.00448.
- [Swischuk et al.(2019)Swischuk, Mainini, Peherstorfer, and Willcox] Renee Swischuk, Laura Mainini, Benjamin Peherstorfer, and Karen Willcox. Projection-based model reduction: Formulations for physics-based machine learning. *Computers & Fluids*, 179:704–717, 2019. doi:10.1016/j.compfluid.2018.07.021.
- [Ionita and Antoulas(2014)] A. C. Ionita and A. C. Antoulas. Data-driven parametrized model reduction in the Loewner framework. *SIAM Journal on Scientific Computing*, 36(3):A984–A1007, 2014. doi:10.1137/130914619.
- [Peherstorfer et al.(2017)Peherstorfer, Gugercin, and Willcox] Benjamin Peherstorfer, Serkan Gugercin, and Karen Willcox. Data-driven reduced model construction with time-domain Loewner models. *SIAM Journal on Scientific Computing*, 39(5):A2152–A2178, 2017. doi:10.1137/16M1094750.
- [Antoulas et al.(2016)Antoulas, Gosea, and Ionita] A. C. Antoulas, I. V. Gosea, and A. C. Ionita. Model reduction of bilinear systems in the loewner framework. *SIAM Journal on Scientific Computing*, 38(5):B889–B916, 2016. doi:10.1137/15M1041432.
- [Gosea and Antoulas(2018)] I. V. Gosea and A. C. Antoulas. Data-driven model order reduction of quadratic-bilinear systems. *Numerical Linear Algebra with Applications*, 25(6):e2200, 2018. doi:https://doi.org/10.1002/nla.2200.
- [Rowley et al.(2009)Rowley, Mezić, Bagheri, Schlatter, and Henningson] Clarence W. Rowley, Igor Mezić, Shervin Bagheri, Philipp Schlatter, and Dan S. Henningson. Spectral analysis of nonlinear flows. *J. Fluid Mech.*, 641: 115–127, 2009. doi:10.1017/S0022112009992059.
- [Schmid(2010)] Peter J. Schmid. Dynamic mode decomposition of numerical and experimental data. *Journal of Fluid Mechanics*, 656:5–28, 2010. doi:10.1017/S0022112010001217.
- [Williams et al.(2015)Williams, Kevrekidis, and Rowley] Matthew O. Williams, Ioannis G. Kevrekidis, and Clarence W. Rowley. A data-driven approximation of the Koopman operator: extending dynamic mode decomposition. *J. Nonlinear Sci.*, 25(6):1307–1346, 2015. doi:10.1007/s00332-015-9258-5.
- [Brunton et al.(2016)Brunton, Proctor, and Kutz] Steven L. Brunton, Joshua L. Proctor, and J. Nathan Kutz. Discovering governing equations from data by sparse identification of nonlinear dynamical systems. *Proceedings of the National Academy of Sciences*, 113(15):3932–3937, 2016. doi:10.1073/pnas.1517384113.
- [Loiseau and Brunton(2018)] Jean-Christophe Loiseau and Steven L. Brunton. Constrained sparse Galerkin regression. *J. Fluid Mech.*, 838:42–67, 2018. doi:10.1017/jfm.2017.823.
- [Schaeffer et al.(2018)Schaeffer, Tran, and Ward] Hayden Schaeffer, Giang Tran, and Rachel Ward. Extracting sparse high-dimensional dynamics from limited data. *SIAM Journal on Applied Mathematics*, 78(6):3279–3295, 2018.
- [Hesthaven and Ubbiali(2018)] J.S. Hesthaven and S. Ubbiali. Non-intrusive reduced order modeling of nonlinear problems using neural networks. *Journal of Computational Physics*, 363:55–78, 2018. doi:10.1016/j.jcp.2018.02.037.
- [Wang et al.(2019)Wang, Hesthaven, and Ray] Qian Wang, Jan S. Hesthaven, and Deep Ray. Non-intrusive reduced order modeling of unsteady flows using artificial neural networks with application to a combustion problem. *Journal of Computational Physics*, 384:289–307, 2019. doi:10.1016/j.jcp.2019.01.031.
- [Peherstorfer and Willcox(2016)] Benjamin Peherstorfer and Karen Willcox. Data-driven operator inference for non-intrusive projection-based model reduction. *Computer Methods in Applied Mechanics and Engineering*, 306:196 – 215, 2016. ISSN 0045-7825. doi:10.1016/j.cma.2016.03.025.

- [Kramer and Willcox(2019)] Boris Kramer and Karen E. Willcox. Nonlinear model order reduction via lifting transformations and proper orthogonal decomposition. *AIAA Journal*, 57(6):2297–2307, 2019. doi:10.2514/1.J057791.
- [Qian et al.(2020)Qian, Kramer, Peherstorfer, and Willcox] E. Qian, B. Kramer, B. Peherstorfer, and K. Willcox. Lift & learn: Physics-informed machine learning for large-scale nonlinear dynamical systems. *Physica D: Nonlinear Phenomena*, 406:132401, 2020.
- [Benner et al.(2020a)Benner, Goyal, Kramer, Peherstorfer, and Willcox] Peter Benner, Pawan Goyal, Boris Kramer, Benjamin Peherstorfer, and Karen Willcox. Operator inference for non-intrusive model reduction of systems with non-polynomial nonlinear terms. *Computer Methods in Applied Mechanics and Engineering*, 372:113433, 2020a. doi:10.1016/j.cma.2020.113433.
- [McQuarrie et al.(2021)McQuarrie, Huang, and Willcox] Shane A. McQuarrie, Cheng Huang, and Karen E. Willcox. Data-driven reduced-order models via regularised Operator Inference for a single-injector combustion process. *Journal of the Royal Society of New Zealand*, 0(0):1–18, 2021. doi:10.1080/03036758.2020.1863237.
- [Swischuk et al.(2020)Swischuk, Kramer, Huang, and Willcox] Renee Swischuk, Boris Kramer, Cheng Huang, and Karen Willcox. Learning physics-based reduced-order models for a single-injector combustion process. *AIAA Journal*, 58(6):2658–2672, 2020. doi:10.2514/1.J058943.
- [Benner et al.(2020b)Benner, Goyal, Heiland, and Duff] Peter Benner, Pawan Goyal, Jan Heiland, and Igor Pontes Duff. Operator inference and physics-informed learning of low-dimensional models for incompressible flows. e-prints 2010.06701, arXiv, 2020b. URL arxiv.org/abs/2010.06701. math.NA.
- [Yildiz et al.(2020)Yildiz, Goyal, Benner, and Karasözen] S. Yıldız, P. Goyal, P. Benner, and B. Karasözen. Data-driven learning of reduced-order dynamics for a parametrized shallow water equation. *arXiv preprint arXiv:2007.14079*, 2020.
- [Qian et al.(2021)Qian, Farcas, and Willcox] Elizabeth Qian, Ionut-Gabriel Farcas, and Karen Willcox. Reduced operator inference for nonlinear partial differential equations, 2021.
- [Gosea and Duff(2020)] Ion Victor Gosea and Igor Pontes Duff. Toward fitting structured nonlinear systems by means of dynamic mode decomposition, 2020.
- [Chorin and Stinis(2006)] Alexandre Chorin and Panagiotis Stinis. Problem reduction, renormalization, and memory. *Commun. Appl. Math. Comput. Sci.*, 1(1):1–27, 2006. doi:10.2140/camcos.2006.1.1.
- [Givon et al.(2004)Givon, Kupferman, and Stuart] Dror Givon, Raz Kupferman, and Andrew Stuart. Extracting macroscopic dynamics: model problems and algorithms. *Nonlinearity*, 17(6):R55–R127, 2004. doi:10.1088/0951-7715/17/6/r01.
- [Gouasmi et al.(2017)Gouasmi, Parish, and Duraisamy] Ayoub Gouasmi, Eric J. Parish, and Karthik Duraisamy. A priori estimation of memory effects in reduced-order models of nonlinear systems using the More & Zwanzig formalism. *Proceedings of the Royal Society A: Mathematical, Physical and Engineering Sciences*, 473(2205):20170385, 2017. doi:10.1098/rspa.2017.0385.
- [Mou et al.(2021)Mou, Koc, San, Rebholz, and Iliescu] Changhong Mou, Birgul Koc, Omer San, Leo G. Rebholz, and Traian Iliescu. Data-driven variational multiscale reduced order models. *Computer Methods in Applied Mechanics and Engineering*, 373:113470, 2021. doi:<https://doi.org/10.1016/j.cma.2020.113470>.
- [Fick et al.(2018)Fick, Maday, Patera, and Taddei] Lambert Fick, Yvon Maday, Anthony T. Patera, and Tommaso Taddei. A stabilized pod model for turbulent flows over a range of reynolds numbers: Optimal parameter sampling and constrained projection. *Journal of Computational Physics*, 371:214–243, 2018. doi:10.1016/j.jcp.2018.05.027.
- [Rahman et al.(2019)Rahman, Ahmed, and San] Sk. M. Rahman, S. E. Ahmed, and O. San. A dynamic closure modeling framework for model order reduction of geophysical flows. *Physics of Fluids*, 31(4):046602, 2019. doi:10.1063/1.5093355.
- [Wang et al.(2020)Wang, Ripamonti, and Hesthaven] Qian Wang, Nicolò Ripamonti, and Jan S. Hesthaven. Recurrent neural network closure of parametric pod-galerkin reduced-order models based on the Mori-Zwanzig formalism. *Journal of Computational Physics*, 410:109402, 2020. ISSN 0021-9991. doi:<https://doi.org/10.1016/j.jcp.2020.109402>.
- [Peherstorfer(2020)] B. Peherstorfer. Sampling low-dimensional Markovian dynamics for pre-asymptotically recovering reduced models from data with operator inference. *SIAM Journal on Scientific Computing*, 42(5):A3489–A3515, 2020. doi:10.1137/19M1292448.

- [Tan Uy and Peherstorfer(2020)] Wayne Isaac Tan Uy and Benjamin Peherstorfer. Probabilistic error estimation for non-intrusive reduced models learned from data of systems governed by linear parabolic partial differential equations. *arXiv e-prints*, art. arXiv:2005.05890, May 2020.
- [Uy and Peherstorfer(2021)] Wayne Isaac Tan Uy and Benjamin Peherstorfer. Operator inference of non-markovian terms for learning reduced models from partially observed state trajectories, 2021.
- [Goyal and Benner(2021)] Pawan Goyal and Peter Benner. Lqresnet: A deep neural network architecture for learning dynamic processes, 2021.
- [Bistrian and Navon(2015)] D. A. Bistrian and I. M. Navon. An improved algorithm for the shallow water equations model reduction: Dynamic Mode Decomposition vs POD. *International Journal for Numerical Methods in Fluids*, 78(9):552–580, 2015. doi:10.1002/fld.4029.
- [Bistrian and Navon(2017)] Diana Alina Bistrian and Ionel Michael Navon. Randomized dynamic mode decomposition for nonintrusive reduced order modelling. *Internat. J. Numer. Methods Engrg.*, 112(1):3–25, 2017. doi:10.1002/nme.5499.
- [Esfahanian and Ashrafi(2009)] Vahid Esfahanian and Khosro Ashrafi. Equation-free/Galerkin-free reduced-order modeling of the shallow water equations based on Proper Orthogonal Decomposition. *Journal of Fluids Engineering*, 131(7):071401–071401–13, 2009. doi:10.1115/1.3153368.
- [Karasözen et al.(2021)Karasözen, Yıldız, and Uzunca] Bülent Karasözen, Süleyman Yıldız, and Murat Uzunca. Structure preserving model order reduction of shallow water equations. *Mathematical Methods in the Applied Sciences*, 44(1):476–492, 2021. doi:10.1002/mma.6751.
- [Lozovskiy et al.(2016)Lozovskiy, Farthing, Kees, and Gildin] Alexander Lozovskiy, Matthew Farthing, Chris Kees, and Eduardo Gildin. POD-based model reduction for stabilized finite element approximations of shallow water flows. *Journal of Computational and Applied Mathematics*, 302:50 – 70, 2016. ISSN 0377-0427. doi:10.1016/j.cam.2016.01.029.
- [Lozovskiy et al.(2017)Lozovskiy, Farthing, and Kees] Alexander Lozovskiy, Matthew Farthing, and Chris Kees. Evaluation of Galerkin and Petrov-Galerkin model reduction for finite element approximations of the shallow water equations. *Computer Methods in Applied Mechanics and Engineering*, 318:537 – 571, 2017. doi:10.1016/j.cma.2017.01.027.
- [Ahmed et al.(2020)Ahmed, San, Bistrian, and Navon] Shady E. Ahmed, Omer San, Diana A. Bistrian, and Ionel M. Navon. Sampling and resolution characteristics in reduced order models of shallow water equations: Intrusive vs nonintrusive. *International Journal for Numerical Methods in Fluids*, 92(8):992–1036, 2020. doi:10.1002/fld.4815.
- [Ştefănescu et al.(2014)Ştefănescu, Sandu, and Navon] Răzvan Ştefănescu, Adrian Sandu, and Ionel M Navon. Comparison of POD reduced order strategies for the nonlinear 2D shallow water equations. *International Journal for Numerical Methods in Fluids*, 76(8):497–521, 2014.
- [Benner et al.(2018)Benner, Goyal, and Gugercin] P. Benner, P. Goyal, and S. Gugercin. ℓ_2 -quasi-optimal model order reduction for quadratic-bilinear control systems. *SIAM Journal on Matrix Analysis and Applications*, 39(2): 983–1032, 2018. doi:10.1137/16M1098280.
- [Benner and Goyal(2021)] Peter Benner and Pawan Goyal. Interpolation-based model order reduction for polynomial systems. *SIAM Journal on Scientific Computing*, 43(1):A84–A108, 2021. doi:10.1137/19M1259171.
- [Leva(2008)] P. d. Leva. MULTIPROD TOOLBOX, multiple matrix multiplications, with array expansion enabled. Technical report, University of Rome Foro Italico, Rome, 2008.
- [Salmon(2007)] R. Salmon. A general method for conserving energy and potential enstrophy in shallow-water models. *Journal of the Atmospheric Sciences*, 64(2):515–531, 2007. doi:10.1175/JAS3837.1.
- [Stewart and Dellar(2016)] Andrew L. Stewart and Paul J. Dellar. An energy and potential enstrophy conserving numerical scheme for the multi-layer shallow water equations with complete Coriolis force. *Journal of Computational Physics*, 313:99 – 120, 2016. doi:10.1016/j.jcp.2015.12.042.
- [Zeitlin(2018)] Vladimir Zeitlin. *Geophysical fluid dynamics: understanding (almost) everything with rotating shallow water models*. Oxford University Press, Oxford, 2018. doi:10.1093/oso/9780198804338.001.0001.
- [Dellar(2002)] Paul J. Dellar. Hamiltonian and symmetric hyperbolic structures of shallow water magnetohydrodynamics. *Physics of Plasmas*, 9(4):1130–1136, 2002. doi:10.1063/1.1463415.
- [Kahan(1993)] W. Kahan. Unconventional numerical methods for trajectory calculations. Technical report, Computer Science Division and Department of Mathematics, University of California, Berkeley, 1993. Unpublished lecture notes.

- [Celledoni et al.(2015)] Celledoni, McLachlan, McLaren, Owren, and Quispel] Elena Celledoni, Robert I. McLachlan, David I. McLaren, Brynjulf Owren, and G. R. W. Quispel. Discretization of polynomial vector fields by polarization. *Proceedings of the Royal Society of London A: Mathematical, Physical and Engineering Sciences*, 471(2184), 2015. doi:10.1098/rspa.2015.0390.
- [Celledoni et al.(2013)] Celledoni, McLachlan, Owren, and Quispel] Elena Celledoni, Robert I. McLachlan, Brynjulf Owren, and G R W Quispel. Geometric properties of Kahan’s method. *Journal of Physics A: Mathematical and Theoretical*, 46(2):025201, 2013. URL <http://stacks.iop.org/1751-8121/46/i=2/a=025201>.
- [Eidnes et al.(2019)] Eidnes, Li, and Sato] S. Eidnes, L. Li, and S. Sato. Linearly implicit structure-preserving schemes for Hamiltonian systems. *Journal of Computational and Applied Mathematics*, page 112489, 2019. doi:10.1016/j.cam.2019.112489.
- [Benner and Feng(2015)] Peter Benner and Lihong Feng. Model order reduction for coupled problems. *Appl Comput Math Int J*, 14:3–22, 01 2015.
- [Reis and Stykel(2007)] Timo Reis and Tatjana Stykel. Stability analysis and model order reduction of coupled systems. *Math. Comput. Model. Dyn. Syst.*, 13(5):413–436, 2007. doi:10.1080/13873950701189071.
- [Halko et al.(2011)] Halko, Martinsson, and Tropp] N. Halko, P. G. Martinsson, and J. A. Tropp. Finding structure with randomness: Probabilistic algorithms for constructing approximate matrix decompositions. *SIAM Review*, 53(2):217–288, 2011. doi:10.1137/090771806.
- [Bach et al.(2019)] Bach, Ceglia, Song, and Duddeck] C. Bach, D. Ceglia, L. Song, and F. Duddeck. Randomized low-rank approximation methods for projection-based model order reduction of large nonlinear dynamical problems. *International Journal for Numerical Methods in Engineering*, 118(4):209–241, 2019. doi:10.1002/nme.6009.
- [Benner and Breiten(2015)] P. Benner and T. Breiten. Two-sided projection methods for nonlinear model order reduction. *SIAM Journal on Scientific Computing*, 37(2):B239–B260, 2015. doi:10.1137/14097255X.
- [Martins and Hwang(2013)] Joaquim R. R. A. Martins and John T. Hwang. Review and unification of methods for computing derivatives of multidisciplinary computational models. *AIAA Journal*, 51(11):2582–2599, 2013. doi:10.2514/1.J052184.
- [Tikhonov and Arsenin(1977)] Andrey N. Tikhonov and Vasilii Y. Arsenin. *Solutions of ill-posed problems*. V. H. Winston & Sons, 1977.
- [Hansen(1987)] Per Christian Hansen. The truncatedsvd as a method for regularization. *BIT Numerical Mathematics*, 27(4):534–553, 1987. doi:10.1007/BF01937276.
- [Hansen(2000)] P. C. Hansen. The l-curve and its use in the numerical treatment of inverse problems. In *Computational Inverse Problems in Electrocardiology*, ed. P. Johnston, *Advances in Computational Bioengineering*, pages 119–142. WIT Press, 2000.
- [Ohlberger and Rave(2016)] Mario Ohlberger and Stephan Rave. Reduced basis methods: Success, limitations and future challenges. *Proceedings of the Conference Algoritmy*, pages 1–12, 2016.
- [Mou et al.(2020)] Mou, Liu, Wells, and Iliescu] Changhong Mou, Honghu Liu, David R. Wells, and Traian Iliescu. Data-driven correction reduced order models for the quasi-geostrophic equations: a numerical investigation. *International Journal of Computational Fluid Dynamics*, 34(2):147–159, 2020. doi:10.1080/10618562.2020.1723556.
- [Jin et al.(2020)] Jin, Zhang, Zhu, Tang, and Karniadakis] Pengzhan Jin, Zhen Zhang, Aiqing Zhu, Yifa Tang, and George Em Karniadakis. Sympnets: Intrinsic structure-preserving symplectic networks for identifying hamiltonian systems. *Neural Networks*, 132:166–179, 2020. ISSN 0893-6080. doi:10.1016/j.neunet.2020.08.017.